

New constraints on sterile neutrino dark matter from the Galactic Center

R. Yunis,^{a,b} C. R. Argüelles,^c Nick E. Mavromatos,^d A. Moliné,^e A. Krut,^{a,b,f} J. A. Rueda,^{a,b,g} R. Ruffini^{a,b,g}

^aICRANet, Piazza della Repubblica 10, I-65122 Pescara, Italy

^bDipartimento di Fisica and ICRA, Sapienza Università di Roma, P.le Aldo Moro 5, I-00185 Rome, Italy

^cInstituto de Astrofísica de La Plata (CCT La Plata, CONICET, UNLP), Paseo del Bosque, B1900FWA La Plata, Argentina

^dTheoretical Particle Physics and Cosmology Group, Department of Physics, King's College London, Strand WC2R 2LS, London, U.K.

^eInstituto de Astrofísica e Ciências do Espaço, Faculdade de Ciências da Universidade de Lisboa, Edifício C8, Campo Grande, P-1749-016 Lisbon, Portugal

^fUniversity of Nice-Sophia Antipolis, 28 Av. de Valrose, 06103 Nice Cedex 2, France

^gICRANet-Rio, CBPF, Rua Dr. Xavier Sigaud 150, Rio de Janeiro, RJ, 22290-180, Brazil

E-mail: rafael.yunis@icranet.org

Abstract. We calculate the most stringent constraints up to date on the parameter space for sterile neutrino warm dark matter models possessing a radiative decay channel into X-rays. These constraints arise from the X-ray flux observations from the Galactic center (central parsec), taken by the XMM and NuSTAR missions. We compare the results obtained from using different dark matter density profiles for the Milky Way, such as NFW, Burkert or Einasto, to that produced by the Ruffini-Argüelles-Rueda (RAR) fermionic model, which has the distinct feature of depending on the particle mass. We show that due to the novel core-halo morphology present in the RAR profile, the allowed particle mass window is narrowed down to $m_s \sim 10 - 15$ keV, when analyzed within the ν MSM sterile neutrino model. We further discuss on the possible effects in the sterile neutrino parameter-space bounds due to a self-interacting nature of the dark matter candidates.

Contents

1	Introduction	1
2	Sterile neutrino decay: X-ray flux	3
2.1	DM halo density profiles	5
2.2	RAR profile	6
3	Signal analysis	8
3.1	Galactic Center	8
3.2	0-bounce photons	11
4	Parameter space bounds	14
4.1	Galactic Center	14
4.2	0-bounce photons	16
4.3	ν MSM parameter bounds from other sources	16
4.4	Comparison with recent works	18
5	Parameter space relaxation & dark sector interactions	18
5.1	Vector Interactions among sterile neutrinos	19
6	Conclusions	22
A	S factor	24
B	A sterile neutrino production mechanism: V-boson decay	25

1 Introduction

While the evidence for the existence of dark matter (DM) is implied from astrophysical and cosmological observations of gravitational effects, a huge effort is still focused on the understanding of the nature of the particles that make up this unknown matter as well as its detection [1–4]. Among the myriad of DM candidates proposed, a sterile neutrino with a mass in the keV range has been claimed as a viable candidate, falling in the category of *warm* DM (WDM) [5–11].

These claims seem to be revitalized given recent results about neutrino oscillations and several other physics phenomenons which are not predicted by the Standard Model (SM) and suggests new, unknown physics [12–15]. In particular, a minimal extension of the SM, the so-called *Neutrino Minimal Standard Model* (ν MSM) introduces three sterile right handed neutrinos, where the lightest one might account for the presence of DM in the universe [10].

From the gravitational evidence about the existence of DM, we can infer that the DM particle must be stable on cosmological time scales. Nevertheless, huge amounts of DM particles can decay even for such extremely long lifetimes and the decay signals may be in the observable range to be detectable [16–43]. Within the framework of the ν MSM, the hypothetical sterile neutrino is an example of decaying DM with a lifetime several times greater than the age of the Universe [10]. Viability for sterile neutrinos as to constitute the

entirety of cosmological DM requires low enough mixing with the standard sector, measured by the *mixing angle*

$$\theta^2 = \sum_{\alpha=e,\mu,\tau} (v^2 F_{\alpha,1})/m_s^2, \quad (1.1)$$

with v^2 the Higgs boson v.e.v., $F_{\alpha,1}$ the Yukawa couplings for the right-chiral neutrinos and m_s the sterile neutrino mass. Indeed, it is enough for θ^2 to fall below $2.5 \times 10^{-13} (\text{MeV}/m_s)^5$ as to have a lifetime longer than the age of the universe for tree-level decays [44]. More stringent observational bounds, as the ones arising from the diffuse X/ γ -ray background, assure the fulfillment of this life/time condition [44], with corresponding bounds falling just outside the upper-right end limits of the parameter space coverage, e.g. fig. 1. Both the sterile neutrino mass m_s , and the mixing angle between active and sterile neutrinos θ , constitute the parameter space for ν MSM regarding DM. Their decay open the possibility of indirectly detecting DM via the identification of such interactions products as photons or neutrinos. Indeed, the sterile neutrinos would have a subdominant radiative decay channel into a photon and a light (mostly active) neutrinos [45, 46]. An important clue for searching for the decay of a sterile neutrino candidate may be coming from the X-ray observation of DM-dominated objects, such as galaxies and clusters of galaxies. The region of the galaxy with the highest DM density is the Milky Way center and constitutes the classical target for DM searches (see e.g. [47] for a compilation of works). The Galactic center (GC) region has been extensively studied in the realm of sterile neutrino DM decays using observations of several X-ray satellites such as Suzaku, Chandra, XMM-Newton (see [48] for a recent review), as well as from the NuSTAR mission [49]. In this paper, we focus on the possibility of detecting the X-ray signal produced in the GC due sterile neutrino decays, and compare among different hosting DM halo profiles.

The several works cited just above were developed to constraint the ν MSM parameter space using X-ray observations from both galactic and extragalactic objects. Such limits come as complementary to the ones imposed by production mechanisms of DM in the early universe, such as non-resonant (Dodelson - Widrow) production [48, 50, 51] and resonant production [51–53]. Other limits to the ν MSM model include phase space distribution bounds, as well as bounds from local group galaxy counts, which exclude masses below several keV [54–56]. While X-ray bounds provide upper limits to the mixing angle θ (between dark and active sector) as a function of particle mass m_s .

The intensity of the DM decay flux expected from a individual halo depends mainly on the DM density distribution inside it. N-body simulations within the Λ CDM paradigm, seem to point towards a single universal description for the the DM halo density profiles, and different parameterizations had been obtained in the literature [57–61]. However, in this work we are interested in sterile neutrinos pertaining to the WDM paradigm with particles decoupling while still relativistic, implying a subsequent free-streaming which damp primordial density fluctuations below a cutoff scale sensitive to the particle mass (see e.g. [62]). For keV-ish particles, such a damping imply a suppression in the power spectrum which goes from $\sim 10\%$ at Mpc scales when compared with the Λ CDM one, and becomes stronger on scales below 10^2 kpc (see [63] for current constraints). One of the main consequences of such a suppression is the difference in morphology of the DM density profiles: while CDM halos (and sub-halos) are cuspy through the center, the WDM ones tend to form cored inner halos for low enough particle masses *below* keV (see e.g. [64]). Nevertheless, in the case of few to several keV, recent high resolution N-body simulations [65] developed to understand the small-scale structure differences between CDM and WDM cosmologies, show that the density profiles in

WDM halos with masses $M \gtrsim 10^{10} M_\odot$ ¹ are indistinguishable from their CDM counterparts, and well fitted by Einasto profiles [61], or even by NFW [64] (though for much larger halo masses in the later). Therefore, in this paper we will compare the Navarro-Frenk-White (NFW) profile [57, 58], the Einasto (EIN) profile [61, 66] and the Burkert (BUR) profile [67], with the recently proposed Ruffini-Argüelles-Rueda (RAR) profile [68, 69] in order to bracket the theoretical uncertainty in the limits from the modeling of the expected DM decay flux of sterile neutrino WDM.

At this point it is important to emphasize that the RAR model may imply a more self-consistent approach to deal with keV WDM particles instead of the use of NFW (or Einasto, etc), given (i) the limitations of N-body numerical resolution below a given radial scale (usually below ~ 10 kpc); and (ii) the fact that for dwarf galaxies the density profile fits clearly deviates from NFW (see e.g. [65]). Besides, the RAR profile presents distinct features that make up qualitative differences in the analysis, such as an explicit particle mass dependence in the profile itself, and a novel high-density (sub-pc) core density working as alternative to the central BH in addition to the outer halo [69] (see section 2.2). We further estimate the upper limits on the sterile neutrino parameter space (θ, m_s) , comparing the X-ray flux observations from the GC against the (DM halo model dependent) theoretical expected one. In particular, we focus on searches with NuSTAR and XMM-Newton satellites which have provided accurate observation of diffuse X-ray emission within the central region of the Galaxy. Recently, such approaches have been undertaken in the literature using NuSTAR data [49] using corona-like regions around the GC, where diffuse photons are included but excluding the very center (where many individual bright X-ray sources can be identified). Interestingly, when diffuse emission from the very few parsecs around SgrA* is included in the analysis, the RAR density spikes (i.e. quantum cores) which are sensitive to the particle mass, imply the more stringent constraints in the (up to date) free parameter space. The main result from such an analysis accounting for RAR profiles, is that the ν MSM free parameter window is significantly reduced or nearly ruled-out. Nevertheless, we point out in section 5 that novel generation mechanisms for sterile neutrinos acting prior to the $\nu_s \rightarrow \nu + \gamma$ process, can relax considerably the ν MSM free parameter space constraints.

In section 2 we describe the calculation of the expected DM decay flux. We summarize the relevant ingredients to compute it and the choice of parameters of the ν MSM. We consider several parameterizations for the DM density profile and discuss its critical role in the expected DM decay flux. Using the X-ray observations from the GC, in section 4 we obtain the upper limits on the sterile neutrino mixing angles as a function of particle mass. In addition, we describe and compare bounds to the ν MSM parameter space from other similar works on the field. In section 5, we discuss the effects in the relaxation of these bounds due to hidden dark sector interactions recently proposed by some of the authors of this work. Finally, in section 6 we draw our conclusions.

2 Sterile neutrino decay: X-ray flux

The radiative sterile neutrino decay channel to a photon and an active neutrino produces a spectral line in the X-ray. The decay width is proportional to $m_s^5 \sin^2(2\theta)$, where θ is typically a small quantity below the electroweak scale, as arising from Cosmic X-ray Background (CXB) constraints [46]. The expected energy flux observed from the decay of a massive neutrino will

¹Less massive WDM halos do start to show systematically lower concentrations respect to CDM ones [65].

depend on both the distance and distribution of DM across the field of view of the detector, as well as on the parameter space (θ, m_s) .

This decay channel is due to mixing between active and sterile sectors under the ν MSM model. The interaction arises due to mass mixing thanks to the addition of a Majorana mass term for the sterile neutrinos, plus a Yukawa Higgs-portal term as:

$$\mathcal{L}_{\text{Yuk}} = F_{\alpha I} \bar{\ell}_\alpha N_{RI} \phi^c + \text{h.c.}, \quad I = 1, 2, 3 \quad (2.1)$$

where ℓ_α are the lepton doublets of the Standard Model (SM), $\alpha = e, \mu, \tau$, $F_{\alpha I}$ are the appropriate Yukawa couplings which relates to the mixing angle θ via eq. (1.1) above, and ϕ^c is the SM conjugate Higgs field, *i.e.* $\phi^c = i\tau_2 \phi^*$ (with τ_2 the 2×2 Pauli matrix), with N_{RI} the three sterile neutrino fields. Further details will be explored in section 5.

If x denotes the linear coordinate along the line of sight (l.o.s.) and $d\Omega$ the solid angle element of the detector field of view, the differential photon flux from a volume element in the galaxy² $x^2 dx d\Omega$, reaching a unit effective area of the detector is proportional to the DM density profile ρ , and given by

$$df = x^2 dx d\Omega \frac{\Gamma}{m_s} \frac{\rho(r)}{4\pi x}, \quad (2.2)$$

since each volume element contains $\rho(r)/m_s$ sterile neutrinos. In the ν MSM, the decay width Γ , is defined as [45, 70]

$$\Gamma = \frac{9}{1024} \frac{\alpha G_F^2}{\pi^4} m_s^5 |\Theta|^2 \quad (2.3)$$

with α the fine-structure constant, $|\Theta|^2 = \sin^2(2\theta)$ and G_F the Fermi constant. The average flux observed in a solid angle is then found by integrating over the ρ along the line of sight connecting the detector and the GC and the solid angle,

$$F = \frac{\Gamma}{4\pi m_s} \int_{\Omega_{\text{l.o.s.}}} d\Omega \int \rho(r(x, \Omega)) dx. \quad (2.4)$$

This expression can be cast as

$$F = \frac{\Gamma}{4\pi m_s} S_{\text{DM}}, \quad (2.5)$$

where the S_{DM} factor contains both the features of the DM profile of interest and the observation details such as the location of the observed region itself. The remaining factor depend exclusively on the particle physics parameters and ν MSM specific decay rates. By asking $F_{\text{max}}^{\text{obs}} \geq F$ with $F_{\text{max}}^{\text{obs}}$ the maximum observed X-ray flux (see section 3), it is possible to place upper limits on the sterile neutrino mixing angle as a function of particle mass, as shown in the picture below. Two main Milky Way observations/DM profile pairs are shown: expected fluxes corresponding to flat core NFW profile (motivated by observations, see [49]) are compared to NuSTAR observation for diffuse light ~ 100 pc around the GC, as reviewed in [49], placing an upper limit on the sterile neutrino mixing angle. In this work, observations of the very inner \sim few pc of the Milky Way were used and compared against RAR profile. An estimate for this upper bound is obtained, resulting in the more stringent limits within the ν MSM parameter space up to date.

² Ignoring general relativistic effects on proper volume integrals.

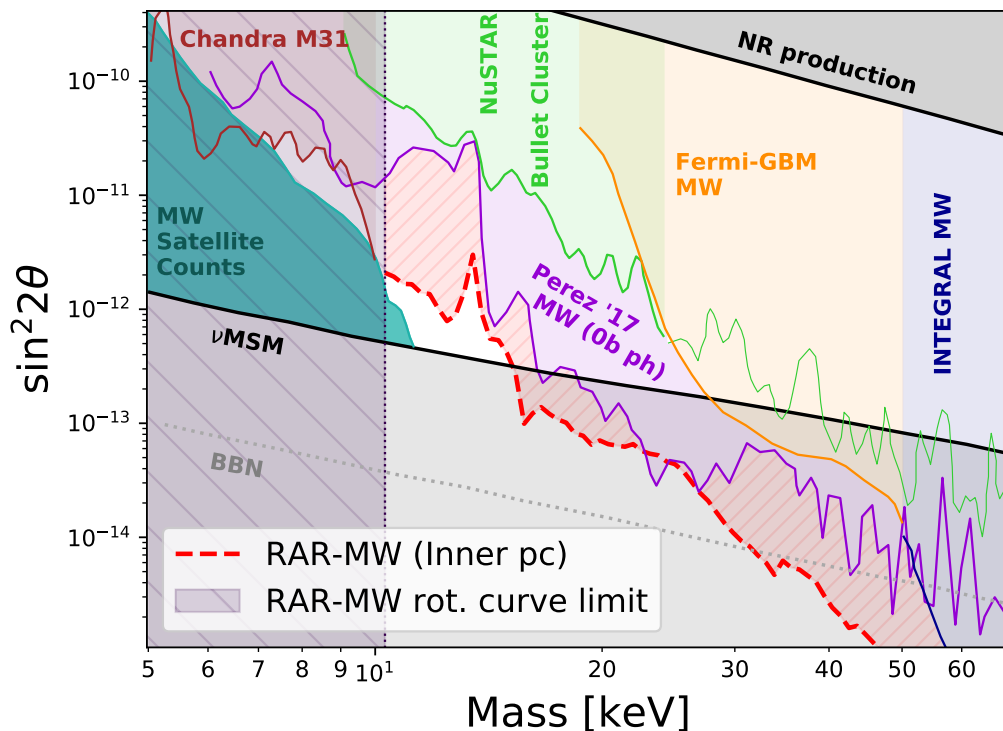


Figure 1. Sterile neutrino parameter space limits obtained for GC observations using RAR profiles, compared to previous bounds. Red-dotted line and 10.4 keV vertical shaded region correspond to RAR limits given by X-ray bounds and MW rotation curve limits [69] respectively. Upper and lower grey shaded regions correspond to production mechanism bounds: NRP under no lepton asymmetry, ν MSM for maximal model produced asymmetry and maximal BBN allowed values [50, 51, 62]. Shaded blue region labels MW satellite count bounds [54, 55]. Other lines refer to several X-ray bounds [55, 71–74] including 0-bounce photon analysis [49], discussed further in section 4.3.

2.1 DM halo density profiles

DM density profiles for galaxy halos have been reviewed by many authors and is still a topic of discussion. As mentioned above, since the expected photon flux from DM decays is proportional to the DM distribution inside the halo, the density profile plays a critical role in DM searches. One of the most commonly used parametrization is the NFW profile [57, 58]

$$\rho_{\text{NFW}}(r) = \frac{\rho_s}{(r/r_s) (1 + (r/r_s))^2}, \quad (2.6)$$

where r_s is the scale radius and ρ_s is the dark matter density at the scale radius. In this work, we consider the local DM density $\rho_{\text{local}} = \rho_{\text{NFW}}(r = r_\odot = 8 \text{ kpc}) = 0.4 \text{ GeV/cm}^3$ and $r_s = 21 \text{ kpc}$, which are compatible with the preferred parameters for the MW halo reviewed in [75].

In order to study the impact of the density profile choice in the calculation of the S factor, we consider other alternative functional forms as the Einasto profile [66],

$$\rho_{\text{EIN}} = \rho_s \exp \left\{ -\frac{2}{\alpha} \left[\left(\frac{r}{r_s} \right)^\alpha - 1 \right] \right\}, \quad (2.7)$$

and the Burkert profile [67],

$$\rho_{\text{BUR}}(r) = \frac{\rho_s}{(1 + r/r_s)^\alpha (1 + r/r_s)^\beta}, \quad (2.8)$$

In this case, our choice is $r_s = 21$ kpc, $\alpha = 0.17$ for the Einasto profile and $r_s = 6$ kpc, $\alpha = 1$ and $\beta = 2$ for the Burkert profile. We also consider for both parametrization the same local DM density as described above.

While DM only simulations of the Milky Way favor profiles with density slopes similar to NFW at small radius, the scenario changes with the addition of baryons. Reference [76], which considered simulated galaxies with baryons that best fit the Milky Way data showed that the density slope is steeper for 1.5 – 6 kpc, and shallower below 1.5 kpc compared to NFW. A conservative approach to this data is considering a density profile identical to NFW, but with constant density below the 1.5 kpc range. We denote this profile as coreNFW. In addition, as complementary to those based on standard cosmological simulations it is possible to obtain the distribution of DM in a halo through a semi-analytical approach, which has the chance to include more rich physical ingredients, such as quantum statistics, thermodynamics, and gravity as we will briefly describe in the next section.

2.2 RAR profile

The recently proposed RAR profile [68] is based on a self gravitating system of massive fermions at finite temperatures. Its formulation and preferred parameters for the MW halo morphology can be seen in [69], as well its implications on MW rotation curve observables from the center to periphery. These profiles carry distinct features that differentiate them from the ones above: first of all have an explicit dependence on fermion mass, a parameter which only appears in the decay rate factor for previous profiles, thus making the S_{DM} factor not completely independent of the decay rate particle model. Also, these types of profiles harbor highly dense compact quantum cores, which are of interest when including the innermost S-star cluster around SgrA*, given that such cores are shown to work as an alternative to the central BH [69].

There are no closed analytical forms for these profiles, but can be integrated from a set of ordinary nonlinear integro-differential equations for different particle masses, with corresponding other free RAR model parameters such as central temperature, degree of central degeneracy and particle escape energy. Interestingly, in [69] it was explicitly shown that there is a unique particle mass range 10.4 – 345 keV such that the RAR continuous solutions are in agreement with the full MW rotation curve (i.e. from $\sim 1 - 5 \times 10^4$ pc), without spoiling the baryonic contribution which dominates at bulge/inner-disk scales (see fig. 2). Moreover, such fermion masses obtained only from rotation curve observables, naturally find sterile neutrino (primordial) candidates from early Universe [10, 77], in agreement with other recent cosmological constraints such Ly- α forest [78, 79], CMB observations and small scale structure (see [48] for a review), among others. The lower end of the mass range (10.4 keV) is obtained under the condition that the total rotation curve (DM+baryons) remains consistent with MW observations, while the upper mass range (345 keV) is the limiting mass before the whole configurations become unstable [69]. The RAR profiles firmly excludes particle masses below the keV range, given that the central (too extended) cores overshoot the observed rotation curve in the bulge region (see fig. 2). Result which is in line with totally independent phase-space (Tremaine&Gunn-like) bounds.

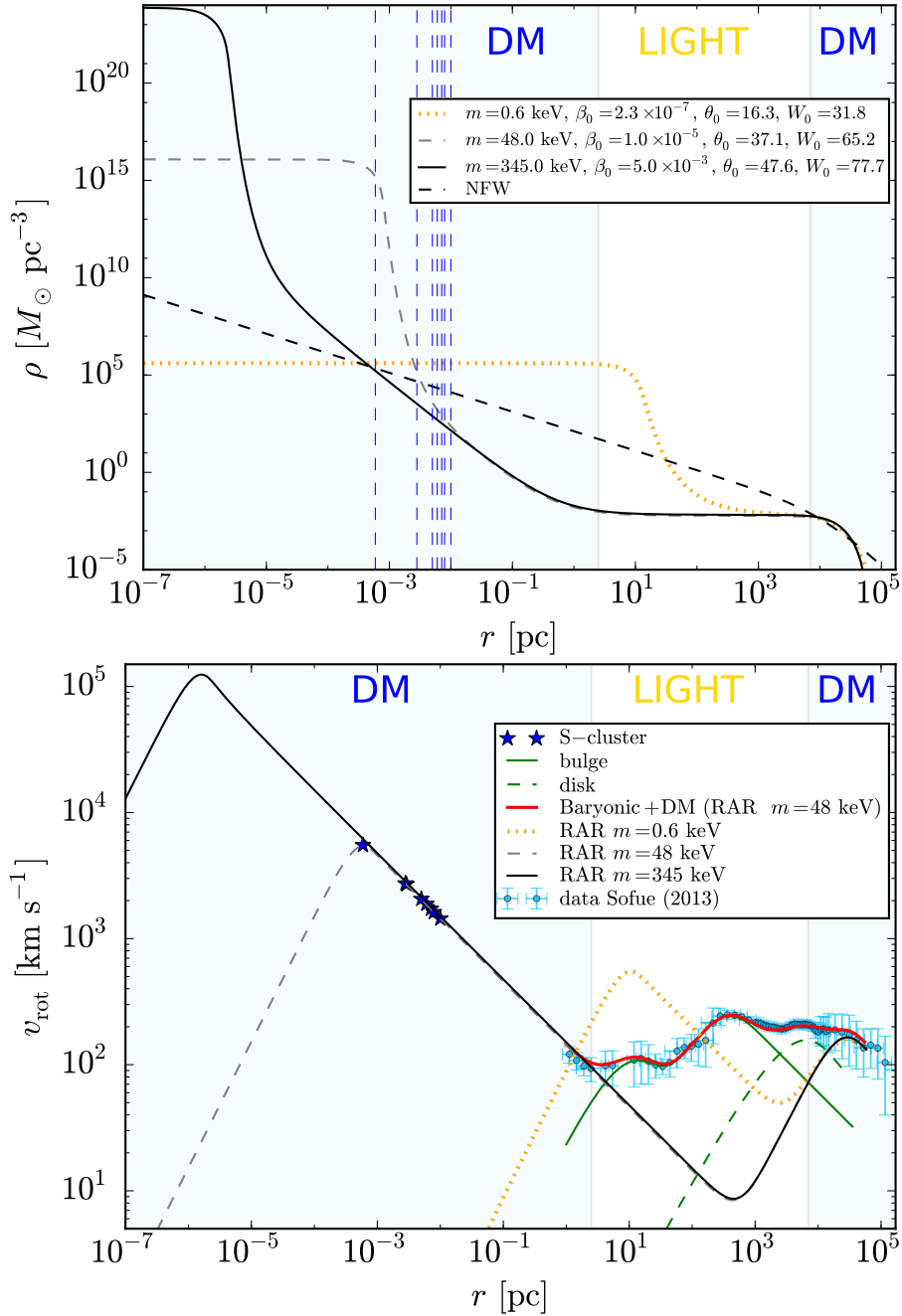


Figure 2. (Color online) Theoretical density profiles and rotation curves from 10^{-7} pc all the way to 10^5 pc, for three representative fermion masses in the $mc^2 \sim \text{keV}$ region: 0.6 keV (dotted yellow curve), 48 keV (long-dashed gray curve) and 345 keV (solid black curve), with corresponding free RAR model parameters: (β_0, θ_0, W_0) reading for central temperature, degeneracy, and escape parameters respectively. The RAR solutions for $mc^2 = 10.4 - 345$ keV are in agreement with the observed rotation curve from pc scales and on (i.e. Sofue-data). For the case of $mc^2 = 48$ keV, we include the total rotation curve (red thick curve) including the total baryonic (bulge + disk) component. The dashed blue lines in upper panel indicate the position of the S-cluster stars [80]. The NFW density profile is shown for sake of comparison as obtained in [81] (dashed black curve). Fig. taken from [69].

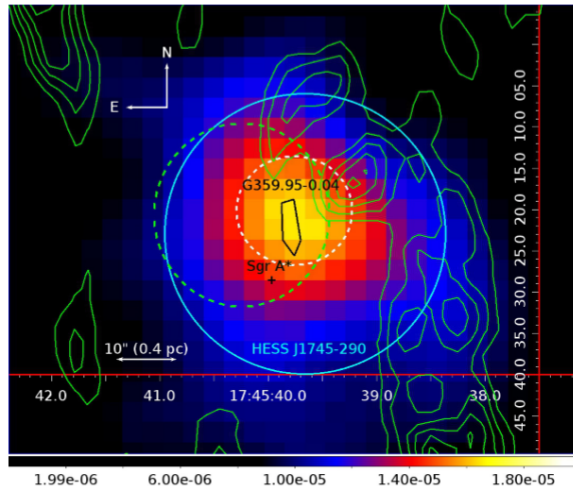


Figure 3. NuSTAR 20 – 40 keV band image zoomed in the central 30 region overlaid with SgrA* (black cross), the centroid of the TeV source HESS J1745 – 290 (cyan circle), PWN candidate G359.95 – 0.04 (black polygon) and circumnuclear disk (green contours). Reproduced from [82] for didactical purposes.

3 Signal analysis

So far we have introduced all the ingredients in order to perform the analytical calculation of the DM decay flux. By comparing the expected flux defined in eq. (2.5) with the observed one (i.e. such that $F_{\max}^{\text{obs}} \geq F$, see Sec. below) it is possible to place upper limits on the sterile neutrino mixing angles as a function of particle mass. In this way, an astrophysical region must be selected, task which is presented in this section from NuSTAR and XMM-Newton observations. The more stringent limits to the θ parameter will come from regions with a low maximal observed flux (i.e. few observed photons) and a high S factor; then a high expected theoretical flux (i.e. high expected photons), as evidenced in eq. (2.5). A suitable selection for the observation region must then fulfill such both conditions.

3.1 Galactic Center

The main conclusions of this work (i.e. most stringent constraints to sterile neutrino parameter space) arise when considering the observations (photon flux) coming from the innermost parsecs of the Galaxy. This observation is centred around G369.95-0.04, which is a Pulsar Wind Nebula candidate located at about less than 9 arcsec away from SgrA*, which we identify as the geometrical center of all DM density profiles here adopted. The observation spans a circular region of 40 arcsec around the centroid of G369.95-0.04. The observational data with corresponding spectra has been obtained by the NuSTAR instrument, as presented in [82].

The spectral analysis of this region shows a rich variety of X-ray sources in the 2 – 40 keV band, according to [82]. Such features include SgrA*, G359.95-0.04, SgrA East, stellar winds, element lines and the CHXE,³ among others.

This is an observation area filled with X-ray sources, and is expected to have a high observed photon flux. Indeed, we have performed such a F_{\max}^{obs} analysis for a set of energies in

³ Central Hard X-ray Emission. According to the detailed spectral study of two nearby intermediate polars and the CHXE by [83], the CHXE emission is likely an unresolved population of massive magnetic cataclysmic variables (CVs).

the range 2 – 50 keV. The results can be seen in fig. 5. We can see a maximal observed photon flux of about $\sim 10^{-2}$ cts s $^{-1}$ m $^{-2}$ for a region of about 4×10^{-4} deg 2 (total solid angle area of a 40 arcsec circle around G359.95-0.04). Interestingly, some DM profiles show a significant density increase at the inner parsecs of the galaxy, which leads to a boost in S_{DM} factor for those regions. RAR profiles are the best example, as the inner compact core accounts for most of the S_{DM} factor contributions, several orders of magnitude above other profiles for the same central area (as seen in following sections).

Maximal line flux

In order to successfully obtain limits on the sterile neutrino DM parameter space from observations, it is necessary to determine a maximum X-ray flux that could have possibly been originated from DM decay.

Null-detection hypothesis has been tested by [49] for the GC region within 10 2 pc from SgrA*.⁴ As this condition is independent from DM halo modeling and relative instrumental errors are unchanged, we assume the hypothesis to hold for the central few pc region as well. Moreover, given the fact that a best fit to the total observed Flux including only astrophysical sources has been obtained [82], using the same instrument and within expected error bounds. A detailed analysis based on the modeling of all the known sources within the central pc, leading (or not) to the explicit null-detection conclusion will appear somewhere.

Currently, observed spectra for the diffuse emission of the GC on the central \sim few pc show features that could all be accounted for with astrophysical sources. Then, decays in the X-ray band could only have fluxes that fall within the statistical uncertainty for the measured spectra. Sterile neutrino decay modes can be approximated as monochromatic within the energy definition of current instrument, so the expected shape of a DM decay line in an observed spectrum would be a Gaussian peak no larger than the 3σ confidence interval on the spectral fit, and with a width determined by the instrument’s energy definition.

Following the criterion used in [84], we approximate the 3σ confidence level for a spectra at a given energy by calculating the confidence intervals of a power law approximation centered around that given energy.

Then, a maximal DM decay line would be seen in the spectra as a Gaussian peak, with a flux not exceeding the spectra plus its 3σ error and as wide as the instrument’s resolution for such energy. This line would give an upper limit for the total DM decay flux, calculated as the integral of such maximal Gaussian peak. As an example, we show one of this maximal peaks for a given energy in fig. 4.

As explained in [49], the expected maximal line flux can be estimated by the following two main factors: the linewidth set by the detector energy resolution, and the maximum allowed contribution of the line to the model, set roughly by the local error of data bins. These methods provide a reasonable and conservative estimation for the DM flux upper limit within an energy range in which spectra are well fit by a continuum model, while remaining independent from spectral fitting of the astrophysical sources.

Such analysis has been performed for the diffuse X-ray emission spectra observed by the NuSTAR and XMM hard X-ray surveys [82]. Making use of the spectra coming from a 40 arcsec region around the GC, we performed this analysis for a set of energies in the range 2 – 50 keV, see fig. 5.

⁴ Namely, using the 0-bounce photon analysis for the GC data as also considered in this paper for comparison purposes.

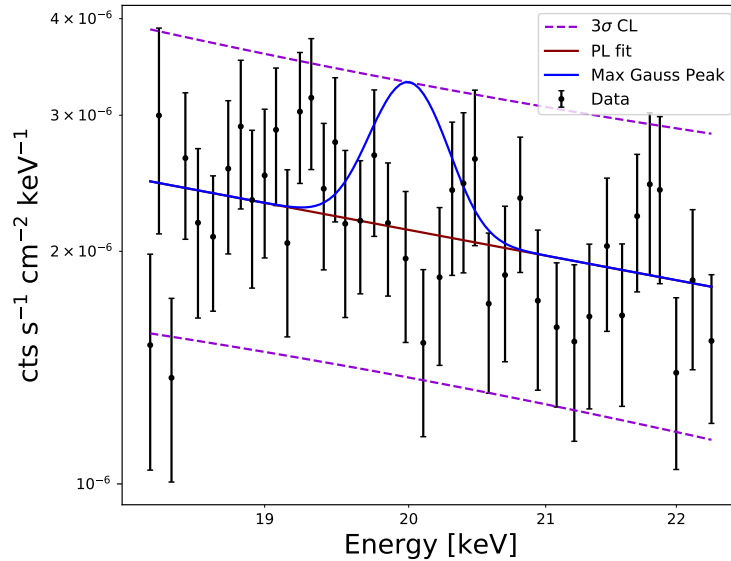


Figure 4. An example of a maximal observed flux analysis for energy 20 keV. We have used the 40 arcsec circular GC region diffuse emission spectra from [82]. The black dots show an example data set, solid lines the power law (PL) and maximal Gaussian peak fits (red and blue respectively) with 3σ confidence bounds for the PL fit on dashed lines.

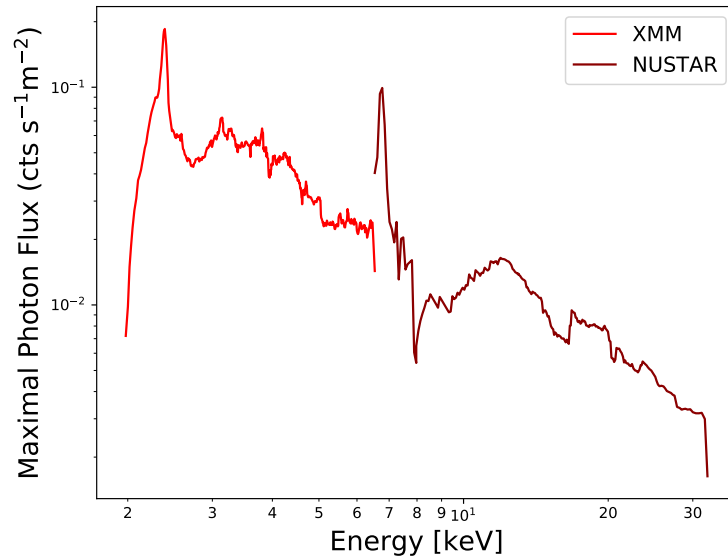


Figure 5. Maximal observed flux bound for the XMM-NuSTAR observation, for 2 – 30 keV range X-ray particle decay. We used the 40 arcsec circular GC region diffuse emission spectra from [82].

The maximal observed flux suffers an enhancement around 6.5 keV, due to the power law approximation of the spectra failing around neutral Fe emission lines [85, 86]. This will lead, in turn, to a bound relaxation in the microscopical model parameter space.

Profile Type	$S_{\text{DM}} [\text{M}_{\odot}\text{pc}^{-2}]$
RAR	7.7904×10^{-2}
NFW	3.6233×10^{-4}
Einasto	3.2055×10^{-4}
Burkert	6.9625×10^{-5}

Table 1. S_{DM} factor values for different profiles types with an integration region of 40 arcsec circular area around the GC. The parameters used for NFW, EIN, BUR profiles are specified in the section 2.1. In the case of RAR profile we consider $mc^2 = 17 \text{ keV}$ and the parameters adopted for the Milky Way halo as in Ref. [69].

S_{DM} estimate

From eqs. (2.4) and (2.5), the S_{DM} factor is obtained integrating over both the direction forming an angle θ with respect to the GC and along the line of sight,

$$S_{\text{DM}} = \int_0^{\infty} \int_{\Omega_{\text{l.o.s.}}} \rho(r(x, \theta)) dx d\Omega, \quad (3.1)$$

where $r(x, \theta) = \sqrt{r_{\odot}^2 + x^2 - 2r_{\odot}x \cos(\theta)}$. We developed a systematic process in order to calculate the S_{DM} factor for each density profile considered in this work. Integration for central-cored profiles requires additional care since numerical processes yield inaccurate results for Dirac delta-like functions. The details about the calculation are discussed in appendix A.

Our results of the S_{DM} factor for the four different profiles are shown in table 1. We define the GC region as a 40 arcsec circular area around the direction of the GC. Integration is performed on the full range of the x coordinate along the line of sight. From that results is clear that the profile choice yields important differences in this factor. As mentioned in the section 2.2, the RAR profiles exhibit compact cores which boost in density on several orders of magnitude at a small radius (where $r < 1 \text{ kpc}$). Thus, we expect a significant contribution in the S_{DM} factor due this small section. In order to quantify such contributions, we systematically calculate S_{DM} factors from ‘donut’ shaped regions of the GC integrating from different θ . We show the results in fig. 6. Profiles were calculated using $m_{\text{fermion}} = 17 \text{ keV}$ as a relevant example within the allowed parameter region in fig. 1.

The S_{DM} factor (thus, the expected decay photon flux) undergoes boosting once the compact core region is included. Clearly from fig. 6, if one neglected this region, the factor would become much smaller with respect to the case of another profiles, thus implying less stringent limits for RAR profiles within these observation target choices.

3.2 0-bounce photons

A different observation region has been considered, this time covering a much larger portion of the observed sky, with fewer X ray luminosity (per solid angle unit). This observation follows the recent works by Perez and collaborators [49] using the NuSTAR mission detectors, but aiming the analysis on the unfocused photons arriving at the detector without passing through the instrument’s focusing optics. When considering pointed observations of the GC, these photons account for the diffuse emission \sim few 100 pc around SgrA*, however, vignetting effects due to physical blocking of the detectors by the instrument itself excludes up to the inner $\sim 150 \text{ pc}$, therefore reducing the astrophysical source contamination, but also removing the inner pc from the observation itself.

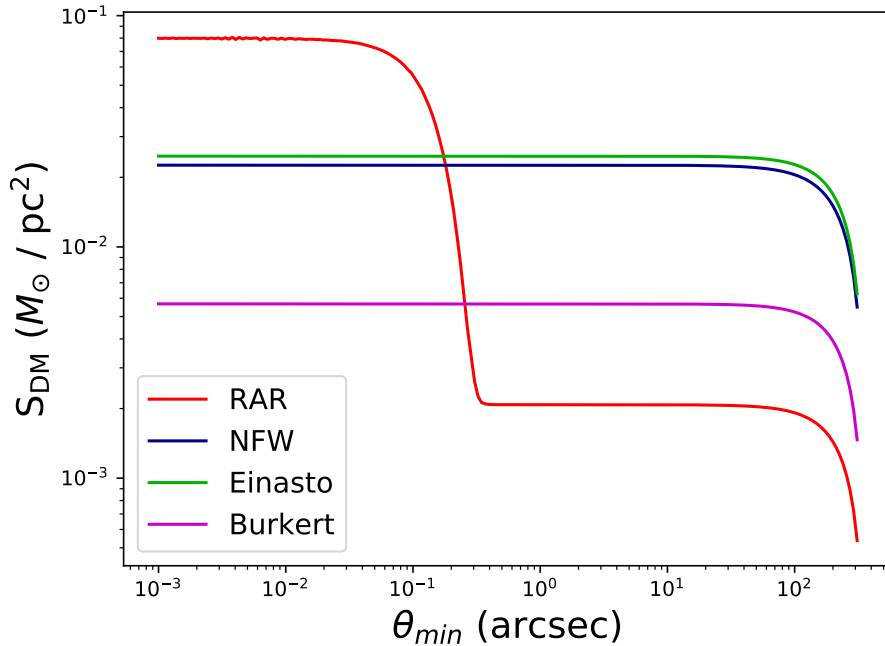


Figure 6. S_{DM} factor for donut regions around the GC as a function of the region’s minimum angle θ_{min} , for 4 different profiles. The maximum angle $\theta_{\text{max}} = 6$ arcmin. NFW, EIN and BUR profiles use the parameter set specified in the text body, RAR profile uses $m_{\text{fermion}} = 17$ keV and parameters fitting the MW halo according to [69].

S_{DM} estimate

For this analysis several observations are considered, roughly centered around the GC, following the procedures in [49]. The total aperture from which these unfocused photons can reach the detector is about 3.5° around the observation center, limited by the aperture stops attached to the focal-plane bench, and partially blocked by the NuSTAR instrument’s optics bench. These introduce both vignetting effects and physical blocking of photons arriving at the detector. Then, certain areas within the observation region are either completely blocked from detection, or the efficiency of the process is significantly diminished. Thus, to account for these effects, an efficiency factor is defined depending on the solid angle coordinates, and the S factor calculations are corrected for detector efficiency in the following form:

$$S_{\text{exp}} = \int_0^\infty \int_{\Omega_{\text{FOV}}} \epsilon(\Omega) \rho(r(x, \Omega)) dx d\Omega, \quad (3.2)$$

with ϵ the detector efficiency factor ranging from 0 to 1.

The shape of the exposure maps for both X-ray detectors on board the NuSTAR mission are obtained in [49, 87]. This sky-exposure correction factor takes into account vignetting effects and obscuration due to the instrument physically blocking photons from entering the detector from certain directions. The exposure map then excludes the inner parsecs of the GC for all observations considered here; a critical factor for dense core DM profiles as explained above.

As an example, we calculated these factors for a Field of View of 4 degrees around the GC, for the exposure map of detector FPMA for observation obsID 40032001002, for three

Profile Type	$S_{\text{DM}} [\text{M}_{\odot}\text{pc}^{-2}]$
RAR	0.3590
NFW	2.0664
coreNFW	1.2546

Table 2. S_{DM} factor values for different profiles types for NuSTAR mission data, using the methods described in [49]. The parameters used for NFW and coreNFW profiles are specified in the section 2.1. In the case of RAR profile we consider $mc^2 = 17 \text{ keV}$ and the parameters adopted for the Milky Way halo as in Ref. [69].

different density profiles, obtaining results as in table 2. We include coreNFW profiles in the analysis following the arguments given in [49].

Due to the exposure map suppressing the contributions from the inner parsecs of the galaxy, RAR S_{DM} factors are significantly suppressed and remain under the ones obtained for NFW and coreNFW. These calculations for the S factor do not include, however, possible contributions from bad pixels or ghost rays (described in [82, 87], for example). These particular features however determine ‘bad data’ regions and should be excluded from the observations and the S factor calculations. Both of these contributions can account for up to 70 % of the S factor, but are constant across profiles up to a 1.5 % standard deviation,⁵ thus remaining as an order of magnitude estimate and allowing to provide comparisons between different dark matter profiles.

Maximal Line Flux

The joint spectra from this analysis can be seen in [49] for both detectors on board the NuSTAR mission: FPMA and FPMB, as well as an in depth analysis for these signals: a recount of the astrophysical sources considered in the spectral fitting and details on the spectral reduction methods.

We have performed the maximal expected flux analysis for the combined FPMA+FPMB spectra, and the results can be found in fig. 7. The expected flux is about a few $\text{cts s}^{-1}\text{m}^{-2}$, coming from a larger region of about 4 deg^2 total solid angle area.

This method of flux constraining, while it does not depend on spectral fitting models, result in overestimations when comparing with other fit dependent methods of up to a factor of a few.

To outline quantitative differences between this method and other fit-dependent ones we compared with the results on maximal line flux obtained by [49]. A 28.7 % mean difference excess between methods was observed within the full 3 – 25 keV spectral range.

It is important to stress that an overestimation of the observed line flux leads to a relaxation in observational limits (which follows directly from eq. (4.2)) and can only result in more conservative limits for the mixing angle θ . Thus, if our limits to the parameter space using RAR profiles (as exposed in fig. 1) would have been obtained using source-fit dependent methods in the analysis, it would lower the upper bound due to the method difference mentioned above by an average of $\sim 30 \%$ for this data set.

⁵ Tested for all profiles described in [49].

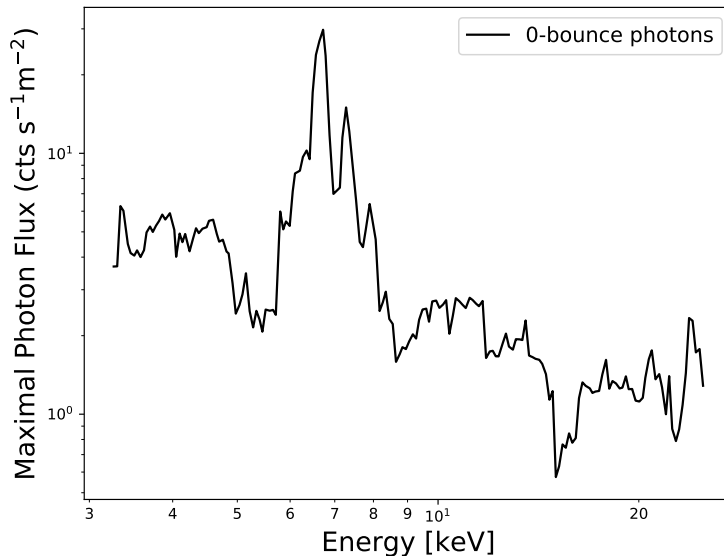


Figure 7. Maximal observed flux bound for the 0-bounce photon observation, for 2 – 30 keV range X-ray particle decay. Used the emission spectra from [49].

4 Parameter space bounds

4.1 Galactic Center

Having established a limit to maximal sterile neutrino decay flux, and having calculated the theoretical expected flux, it is straightforward to obtain a (m_s, θ) parameter space limit. Claiming that the expected flux from DM decay, eq. 2.4, cannot exceed the maximal decay flux coming from X-ray observations (i.e. we assume the null-detection hypothesis for this region):

$$F_{\text{obs}}^{\text{max}} \geq F = \frac{\Gamma}{4\pi m_s} S_{\text{DM}} . \quad (4.1)$$

Recalling the expression for sterile neutrino decay rate given in eq. 2.3, a bound on the mixing angle θ can be obtained as a function of m_s as:

$$\theta^2 \leq 1.9465 \times 10^{-4} \left[\frac{F_{\text{obs}}^{\text{max}}}{\text{ph s}^{-1} \text{cm}^{-2}} \right] \left[\frac{\text{keV}}{m_s} \right]^4 \left[\frac{M_{\odot} \text{pc}^{-2}}{S_{\text{DM}}} \right] \quad (4.2)$$

This X-ray bound becomes more stringent as more accurate constraint on maximum observed flux are achieved. Thus, non observation of DM decay lines on higher resolution equipment or tighter analytical constraints on observed flux, can only contribute to lower the bounds here obtained. The bound is also inversely proportional to S_{DM} , so to obtain tighter constraint it is necessary to identify observational targets with boosted S_{DM} factors for a given DM profile.

We have obtained these bounds for the mixing angle (θ), and for the profiles mentioned above: NFW, Einasto, Burkert and RAR. Results can be seen in fig. 8. Analysis has been performed for the full mass range allowed by the spectra in the case of NFW, EIN and BUR profiles. In the case of RAR type profiles, sterile neutrino masses below 10.4 keV are disallowed, as predicted RAR (central-core) MW rotation curves start to mismatch the inner

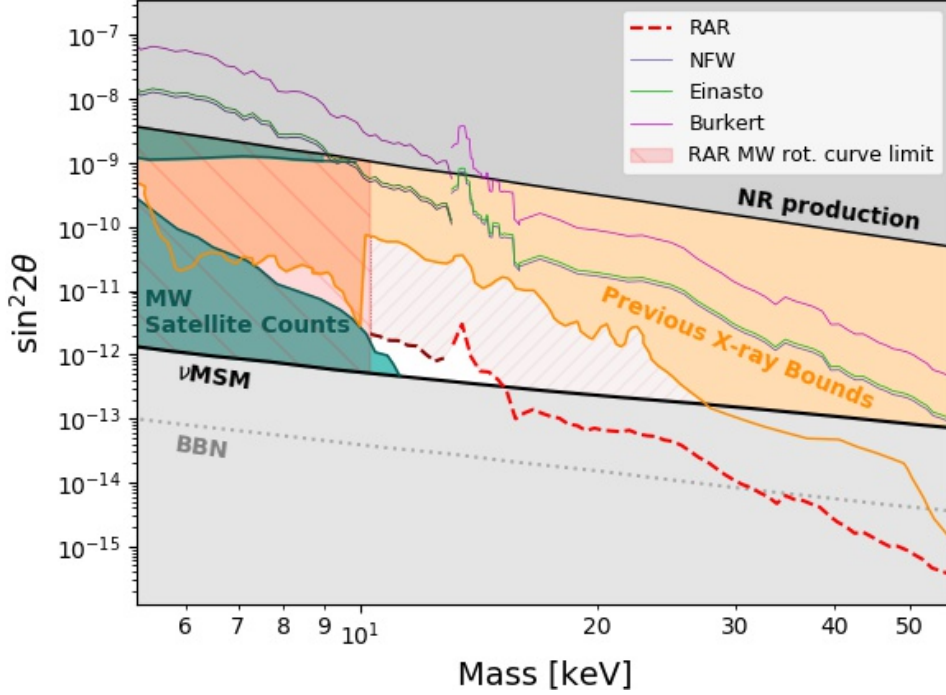


Figure 8. Parameter space limits obtained for GC X-ray emission analysis. Four profile types compared: BUR, EIN, NFW and RAR. 10.4 keV vertical shaded region correspond to RAR limits given by X ray bounds and MW rotation curve limits [69]. Upper and lower grey shaded regions correspond to production mechanism bounds: NRP under no lepton asymmetry, ν MSM for maximal model produced asymmetry and maximal BBN allowed values [50, 51, 62]. Shaded blue region labels MW satellite count bounds [54, 55].

bulge data points (see for example the clear overshooting for the case of $m_s = 0.6$ keV in fig. 2).

As expected, the S_{DM} factor enhancement for the novel core-halo RAR type of profiles results in lower limits in parameter space. As seen before, this enhancement results from the inclusion of the central regions of the GC in the observation, which increases S_{DM} factors and brings them over the ones arising from the other three profiles.

We also analyzed the main contributions to the S_{DM} factor for the RAR profiles. A RAR profile can be split into three distinct features: a compact high density quantum core at $r \lesssim 1$ pc, a baryonic dominated plateau at $r \approx 1 - 10^4$ pc and an outermost halo at $r > 10^4$ pc. We plot the contributions to the X-ray sterile decay limit from profiles comprised only of the core component, core+plateau and a full RAR profile on fig. 9, calculated as $|(\theta_{c/c+p} - \theta)/\theta|$, with $\theta_{c/c+p}$ the limit contributions from core and core+plateau only profiles. We find no significant difference between the limits, thus a S_{DM} factor from GC observation can be approximated by the one obtained from only considering the compact core for RAR profile calculations.

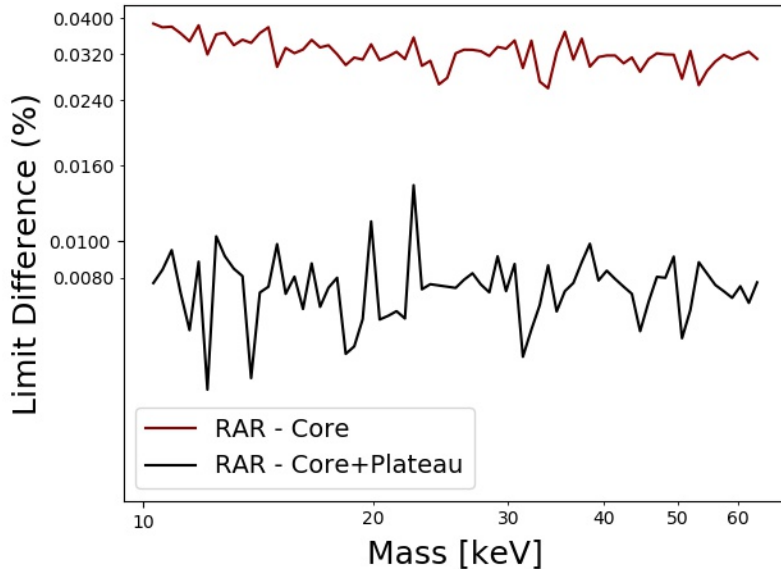


Figure 9. X-ray limit contribution for different sections of RAR profiles, shown as a relative difference between reduced RAR (core and core+plateau) and full RAR profiles.

4.2 0-bounce photons

The parameter-space bound analysis for the 0-bounce photons spectrum is very similar to the one previously mentioned. A few differences reside in the calculation for the S_{DM} factors.

Namely, the exposure map corrections mentioned in previous sections, in addition to averaging over different observations. As the spectrum has been averaged over six observations, and co-added for FPMA and FPMB, each with different exposure maps, the expected flux must be obtained via a weighted average of S_{DM} factors for each one of the observations.

The S_{DM} factor has been calculated as:

$$S_{\text{avg}} = \frac{\sum_i \Delta t \Delta \Omega S_i}{\sum_i \Delta t \Delta \Omega} . \quad (4.3)$$

With Δt the exposure time and $\Delta \Omega$ the effective detector area for each observation. The specific values of these parameters and further observation details can be found in [49].

Once these averages have been taken, the procedure for obtaining a bound for θ are similar to the one taken for the GC. We performed the analysis for profiles NFW and RAR (with parameters previously mentioned), obtaining the results in fig. 10.

The limits for the RAR profile are significantly relaxed for this observation region. This is to be expected, as inner compact regions for these profiles are excluded from the exposure map, therefore not contributing to the S_{DM} factor and thus relaxing the expected bounds.

4.3 ν MSM parameter bounds from other sources

We showed sterile neutrino free-parameter constraints obtained for different regions around the GC, and compared different profiles for each region. All the constraints shown here are upper bounds on the mixing angle as a function of the particle mass, but several other limits exist that limit the parameter space for the particle model under consideration. Phase space density constraints place a lower bound on mass at around 1 – 2 keV, and further X-ray

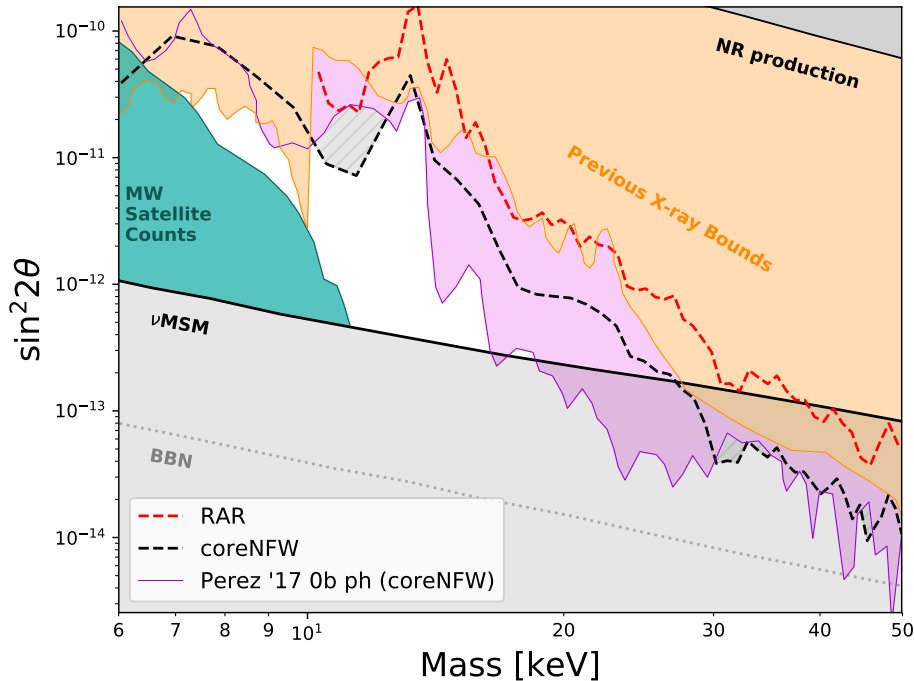


Figure 10. Parameter space limits obtained for 0-bounce photon analysis. Two profile types compared: coreNFW and RAR. Violet line refers to analysis by [49], corresponding to a coreNFW profile.

explorations rule out particle masses above 70 keV (see [49] and references therein). Also, production mechanisms place lower bounds on the mixing angle, leaving a small window of allowed parameter combinations. Recent works [88] provide more stringent lower mass bounds for WDM models based on MW satellite counts, where particle masses lower than 4 keV are strictly ruled out, and suggesting possible future limits for the DM particles around 8 keV.

Lower bounds on the production angle, labeled in the various parameter space plots as ν MSM, BBN and NRP arise from sterile neutrino production mechanisms in the early universe by mixing with the standard sector. These mechanisms are heavily dependent of the values for lepton asymmetry in this early stage: Non-Resonant Production (NRP) [48, 50, 51] mechanisms are the only ones to take place in the absence of asymmetry, and assuming overclosure of the universe a relation between m_s and θ can be plotted in the case of this symmetric universe. The presence of lepton asymmetry adds another available production mechanism: Resonant Production (RP) [51–53]. Part of the DM abundance can be generated in this way, thus relaxing the limits on the mixing angle and allowing lower values. In the context of ν MSM lepton asymmetry can be produced via decays of heavier particles, up to the value that outlines the line labeled as ν MSM in the parameter space plots. If we remain agnostic to the origins of this asymmetry, limits can be further lowered until these values come into conflict with nucleosynthesis predictions, a limit labeled as BBN. Lower bounds arising from production mechanisms are further discussed in section 5, in the context of a minimally-extended ν MSM theory, allowing for a new production mechanism.

4.4 Comparison with recent works

Perez et al. [49] conducted similar searches using 0-bounce photons, and lowered these upper mixing angle bounds further than previous works. In the past sections, we showed that for such analysis and observation region, no stronger limits could be obtained from RAR profiles. However, for observations that include the inner parsecs of the GC, we found that RAR profiles provide stronger limits than NFW counterparts. We then compare the limits obtained for GC observations with the limits obtained by [49] in fig. 1.

RAR profiles for these observations then result in stronger upper bounds for the mixing angle. Under this analysis, the parameter space window for the full ν MSM model is further constrained for RAR profiles. We recall (see discussion in section 3) that fit-dependent maximal observed flux, will certainly set more stringent limits which may completely rule out the ν MSM model, under RAR model assumption for galactic DM.

However, some minimal modifications to the ν MSM which include for interactions in the dark sector, may likely left open the relevance of sterile neutrinos to play the role of the DM in the Universe. Indeed, one should bear in mind that the lowest ν MSM parameter bounds are subject to the sterile neutrino production mechanism, which in turn is sensitive to the adopted rate between lepton-to-baryon asymmetry in the Universe (see [54] for details). For example, if one is agnostic to the generation of lepton asymmetry within ν MSM, then only remains the lower BBN limit, which directly constrains the maximum amount of lepton asymmetry allowed in the Early Universe. Interestingly, novel generation mechanisms for our fermionic candidates beyond ν MSM, will certainly relax such lower bounds, opening the possibility for new sterile neutrino physics as the cosmological DM. Further inspection of these matters are discussed in next section.

5 Parameter space relaxation & dark sector interactions

The above described constraints refer exclusively to the case where the DM fermions are identified with the right handed neutrinos of the ν MSM model [89]. The constraints may be relaxed if (minimal) generalisations of the model are considered, assuming self-interactions among the particles, induced, for instance, by the exchange of massive vector particles in a dark sector of the model. Such an extension was proposed in [90] in an attempt to explain the observed rotation curves (from center to periphery), as well as alleviate discrepancies between observations at galactic (small cosmological) scales and predictions based on numerical simulations based on the Λ CDM model (“small-scale Cosmology crisis”) [91]. Interactions with pseudoscalars (axion-like excitations) in either visible [92] or dark [93, 94] sectors of the pertinent theory have also been considered. In particular, in [92], Yukawa type interactions of right-handed neutrinos with axion pseudoscalars have been proposed as a novel mechanism for generating a Majorana mass for the right handed neutrinos beyond seesaw [95–100], and in this sense they can also be included in the model of [90] in addition to the vector interactions, thus significantly affecting the pertinent constraints.

The presence of such extra ingredients, entail also the important hint that dark matter may consist not only of a dominant component, but of several species, playing a different rôle at various scales. This relaxes significantly constraints on mixing parameters between the DM candidates and Standard Model matter arising from the requirement of avoiding overclosure of the Universe. It is the purpose of this section to discuss briefly several such scenarios and how they modify/relax the constraints pertaining to the ν MSM model of fig. 1.

5.1 Vector Interactions among sterile neutrinos

We commence our discussion by considering the self-interacting DM model of [90]. The relevant Lagrangian is given by :

$$\mathcal{L} = \mathcal{L}_{GR} + \mathcal{L}_{N_{R1}} + \mathcal{L}_V + \mathcal{L}_I \quad (5.1)$$

where

$$\begin{aligned} \mathcal{L}_{GR} &= -\frac{R}{16\pi G}, \\ \mathcal{L}_{N_{R1}} &= i\bar{N}_{R1}\gamma^\mu\nabla_\mu N_{R1} - \frac{1}{2}m\bar{N}_{R1}^c N_{R1}, \\ \mathcal{L}_V &= -\frac{1}{4}V_{\mu\nu}V^{\mu\nu} + \frac{1}{2}m_V^2 V_\mu V^\mu, \\ \mathcal{L}_I &= -g_V V_\mu J_V^\mu = -g_V V_\mu \bar{N}_{R1}\gamma^\mu N_{R1}, \end{aligned} \quad (5.2)$$

with R the Ricci scalar for the metric background, which, for the purposes of [90] which was the study of galactic profiles, it was assumed static and spherically symmetric: $g_{\mu\nu} = \text{diag}(e^\nu, -e^\lambda, -r^2, -r^2 \sin^2 \varphi)$; with e^ν and e^λ functions only of the radial coordinate r , and φ denotes the polar angle. The quantity $\nabla_\mu = \partial_\mu - \frac{i}{8}\omega_\mu^{ab}[\gamma_a, \gamma_b]$ is the gravitational covariant derivative acting on a spinor, with ω_μ^{ab} the spin connection; m is the Majorana mass of the sterile neutrino, whose microscopic origin was left unspecified in [90]. The right-handed sterile neutrinos are denoted by N_{R1} and the superscript ‘ c ’ over a spinor field denotes the charge conjugate, satisfying the Majorana four-spinor condition, $\mathcal{N}^c = \mathcal{N}$ (see [90] for further model details and properties).

For simplicity we assume minimal-coupling of the vector field with the sterile neutrino current J_V^μ in the interaction term \mathcal{L}_I (5.2). This current is conserved if decays of sterile neutrinos are ignored, as done in [90].

Galactic phenomenology accounting for self-interactions as in [90], implies modified Ruffini-Argüelles-Rueda (RAR) profiles (see [68, 69, 101, 102] for standard ones), with *compact core-diluted halo* profiles, including for sufficiently dense cores in order to provide an alternative to massive BHs in agreement with overall rotation curve observations. Such an agreement is acquired for a family of RAR solutions with a corresponding minimum mass of the right handed neutrino about 47 keV (with its maximum allowed mass of about 350 keV, to avoid gravitational collapse). This particle mass based on considerations of the structure of the Milky Way and of other galaxy types, does not fall within the allowed narrow mass range found in this work from an indirect detection analysis within the ν MSM standard scenario. However, when one relaxes the condition that the central quantum core be an alternative to the massive BH scenario, the RAR profiles (either with or without DM self-interactions) can still fit the overall rotation curve in galaxies allowing for lower particle masses down to ~ 10 keV⁶. Importantly, all these results have been obtained assuming a negligible mixing of the sterile neutrino with the SM sector. The case where such a mixing is turned on is discussed in this work through an indirect detection analysis but without allowing for self-interactions

⁶We recall that in [69] it was found that a particle mass in the range 10 – 48 keV is also allowed by the Milky Way rotation curves data. However, in that case the DM quantum core cannot explain the dynamics near the Galactic center so it does not provide an alternative to the BH scenario for SgrA*. In that particle mass range one could consider the DM distribution obtained in a BH+RAR-halo model which could differ near the Galactic center with respect to the one presented in [69]. This calculation is out of the scope of the present work and will be presented elsewhere.

among the DM particles. Possible effects and consequences for the full case including for both kind of interactions (though not solved here) are outlined at the end of this section.

In addition, if one insists that the vector-field-induced self-interactions in the sterile neutrino sector provide solutions to the small-scale cosmology crisis [103], then a strong cross section relative to that of the conventional weak interactions in the SM sector, is required [90]. Indeed, to resolve such tensions between predictions of Λ CDM-based numerical simulations and observations, the self-interacting DM (SIDM) cross section has to be in the range [104]

$$0.1 \leq \frac{\sigma_{\text{SIDM}}/m}{\text{cm}^2 g^{-1}} \leq 0.47, \quad (5.3)$$

according to recent measurements employing novel observables of colliding galaxies. The vector interactions (5.2) in our case, lead to a cross section

$$\sigma_{\text{core}}^{\text{tot}} \approx \frac{(g_V/m_V)^4}{4^3 \pi} 29 m^2 \quad (p^2/m^2 \ll 1). \quad (5.4)$$

which, on account of eq. (5.3), imply for the strength of the vector interaction of the sterile neutrino sector relative to the Fermi coupling G_F of the SM weak interactions [90]

$$\bar{C}_V \equiv \left(\frac{g_V}{m_V} \right)^2 G_F^{-1} \in (2.6 \times 10^8, 7 \times 10^8), \quad (5.5)$$

for ino masses in the range $mc^2 = 47 - 350$ keV, implying that the mass of the massive-vector meson would be constrained to values $m_V \lesssim 3 \times 10^4$ keV, in order to satisfy $g_V \lesssim 1$ as requested by the self-consistency of the perturbation scheme we have applied to compute the cross section by eq. (5.4).⁷

The presence of the vector-sterile-neutrino interaction term \mathcal{L}_I plays an important rôle in the relaxation of the constraints of fig. 1, since it implies an additional production channel for the DM sterile neutrino N_{R1} through the decays of the massive vector field V_μ in the early universe. So, sufficient production of DM may be guaranteed even if one ignores any coupling of sterile neutrinos with the SM sector, by assuming negligible Yukawa couplings $F_{\alpha 1}$ (see eq. (2.1)).

Indeed, as discussed in Appendix, the rate of decay (width Γ) of the vector Boson into a pair of identical Majorana particles (whose mass $\simeq \mathcal{O}(50)$ keV is viewed as negligible when compared to that of the boson V_μ , $m_V \simeq 1 \times 10^4$ keV, according to the phenomenological analysis of [90] in order to reproduce the observed galactic structure) is given approximately at tree level by

$$\Gamma_1 \simeq \frac{g_V^2}{48 \pi} m_V. \quad (5.6)$$

Quantum corrections may affect this result, but will not be the focus of our brief discussion in this work. In models with more than one generation of right handed neutrinos coupled to the vector field there are extra contributions to the total width, which amount to a multiplication of the result in eq. (5.6) by the number of right-handed neutrino flavours N_f (usually $N_f = 3$, like in the case of ν MSM [89]).

The freeze-out temperature of the reaction is estimated by equating Γ_1 in eq. (5.6) with the Hubble parameter H of the Universe, $\Gamma_1 = H$. Assuming standard cosmology, in which

⁷ We recall that for the case of particle masses below 47 keV, as the central core within the RAR model does not provide an alternative to the central BH (see [69, 90]), the above values are somewhat modified.

there is radiation dominance in the Early Universe, the Hubble parameter is expressed in terms the temperature T as [105]

$$H = 1.66 T^2 \mathcal{N}^{1/2} M_{\text{Pl}}^{-1} , \quad (5.7)$$

where \mathcal{N} is the effective number of degrees of freedom of all elementary particles and M_{pl} is the reduced Planck mass. For a minimal extension of the SM, with only right-handed neutrinos and the background B_0 , we may estimate $\mathcal{N} = \mathcal{O}(100)$ at temperatures higher than the electroweak transition. Equating eq. (5.6) with eq. (5.7) we obtain for the pertinent freeze-out temperature, T_D ,

$$T_{D1} \simeq 6.3 \cdot 10^{-2} \frac{|g_V|}{\mathcal{N}^{1/4}} \sqrt{m_V M_{\text{Pl}}} \quad (5.8)$$

As discussed above, the requirement of alleviating the small-scale cosmology crisis via these vector-sterile-neutrino interactions requires [90] $m_V \simeq 10.4 \text{ keV}$, with $g_V = \mathcal{O}(1)$; we then obtain from eq. (5.8) that $T_D = \mathcal{O}(10^8) \text{ GeV}$, which yields the ball park of temperatures in which the sterile neutrino DM abundance is created in our interacting DM model.

The calculation of the sterile-neutrino thermal abundance at the freeze-out can be done as usual by the solution of the pertinent system of Boltzmann equations, or better out of equilibrium thermal field theory techniques (e.g. Kadanoff-Baym equations). In general, one may end up with overproduction of sterile neutrino dark matter that would lead to overclosure of the Universe, unless the would-be freeze-out temperature of the vector mesons lies above the reheating (or even preheating) temperature of the Universe. The latter is not known but it might be constrained by some CMB observations, with a lower limit lying in the range $\sim 20 - 900$ [106, 107]. We observe that in our simplified model the freeze-out temperature in eq. (5.8) is much higher than such lower limits of reheating temperature, and hence overproduction of warm sterile neutrino DM, through the decays of the vector boson, might be achieved. Other ways of avoiding overproduction of DM is via the dilution of the relic right-handed neutrino density by release of entropy through. e.g. decays of the heavier right-handed neutrinos (in models with more than one generation of sterile neutrinos) after their freezeout [108].

The addition to eq. (5.1) of a Yukawa Higgs-portal term as explicated above in eq. (2.1), changes the situation drastically. Indeed, as we already discussed, upon considering such a coupling, one obtains the stringent X-ray and BBN constraints of the mixing angle and mass of N_{R1} depicted in fig. 1, given that eq. (2.1) implies decays of the heavy neutrinos $N_I \rightarrow \nu H$, where H denotes the Higgs excitation field, defined via: $\phi = \langle \phi \rangle + H$. In such a case J_V^μ is *not* conserved in time. However, in the context of ν MSM, the lightest of the heavy neutrinos decay time is longer than the age of the universe [89], hence the latter can be considered as stable for all practical purposes, thus playing the rôle of a DM component.

The thermal history of the Universe in the combined model where both the interaction term (5.2) and the mixing (2.1) is more complicated and we shall not present it here. However, the Dirac Yukawa coupling of the mixing term given by eq. (2.1) for a keV sterile neutrino, of interest here, is sufficiently weak (as required by the seesaw scenarios [95–100] of generating a light active neutrino mass in the SM sector) so it cannot bring the sterile neutrinos into thermal equilibrium above electroweak-scale temperatures. So, in the presence of our vector interactions with a freezeout of order (5.8) they will not play a dominant rôle in the sterile neutrino abundance.

6 Conclusions

We have investigated the X-ray signal expected from the GC due sterile neutrino decays in the energy range $E_\gamma = 2 - 50$ keV. The intensity of the DM decay flux expected from an individual halo depends mainly on the DM density distribution inside it. To discuss in detail the theoretical uncertainties in the calculation, we have estimated the signal assuming different DM densities profiles. Concretely, in section 2 we have described the signal with the decay width defined assuming the ν MSM model and presented different parametrizations such as NFW, Burkert, Einasto. In addition, the RAR profile was considered in the analysis which has the distinct feature of depending on the particle mass. Our results for the S_{DM} factor considering the different profiles are presented in section 3. We conclude that the profile choice yields important differences in this factor as expected. Since the RAR profiles exhibit compact cores which boost in density at small radius we obtain the maximum value for the S_{DM} factor with respect to the other profiles when the compact core region is included. However, we obtain lower values assuming the RAR profile when such regions are not considered in the calculation. The dependence of the S_{DM} factor with the integration of the minimum value of the angle θ_{min} forming with the GC direction, is shown in the fig. 6.

In order to calculate new constraints on the parameter space for sterile neutrino DM models, we compare our analytical results with the X-ray flux observations from the GC and 0-bounce photons taken by the NuSTAR and XMM missions. In section 3 we describe our signal analysis for the GC region (at few pc scales from SgrA*) and also the use of NuSTAR 0-bounce photons (corresponding to $\sim 10^2$ pc off the Galaxy center). We use the NFW and the RAR profile as the representative of our final results about the limits on the mixing angle for sterile neutrino DM in section 4. Assuming that no signal is observed (i.e. we assume a null-detection hypothesis), in eq. (4.2) we discuss the dependencies of the bound respect to m_s , S_{DM} and F_{obs} . For the GC region, the lower limit in the mixing angle is obtained when the RAR profile is considered since the bound is inversely proportional to S_{DM} . Such novel lower bound imply the most stringent constraints up to date on the parameter space, with an allowed particle mass window narrowed down $m_s \sim 10 - 15$ keV within the ν MSM sterile neutrino model (see fig. 1), possessing a radiative decay channel into X rays. The upper one corresponds to the BUR profile (see fig. 8). In the case of use the 0-bounce photons, the RAR profile results in stronger upper bound since the inner compact regions are excluded.

In addition, we further discuss on the possible effects in the sterile neutrino parameter-space bounds due to a self-interacting nature of the dark matter candidates. Self interacting models have been reviewed in section 5, that arise from a generalisation of ν MSM by introducing an exchange of massive vector particles in the dark sector. We briefly consider the implications of such types of models in sterile neutrino physics as cosmological DM, which may circumvent the requirement for universe overclosure, and produce the required DM abundance via dark sector interactions without imposing strong limits to the standard model-dark matter mixing angle θ as those seen in fig. 1.

Acknowledgments

The work of C.R.A is supported by the National Research Council of Science and Technology (CONICET-Argentina). C.R.A and A.M. further acknowledges the hospitality of the ICRANet Headquarters, where finalization of the present work was taking part. The work of N.E.M. is partially supported by the U.K. Science and Technology Facilities Council (STFC) via the

Grant ST/L000258/1. N.E.M. also acknowledges currently the hospitality of IFIC Valencia through a Scientific Associateship (*Doctor Vinculado*). A.K. is supported by the Erasmus Mundus Joint Doctorate Program by Grants Number 2014–0707 from the agency EACEA of the European Commission. The research of A.M. is supported by Fundação para a Ciência e a Tecnologia (FCT) through national funds (UID/FIS/04434/2013) and by FEDER through COMPETE2020 (POCI-01-0145-FEDER-007672).

A S factor

An algorithm was developed to perform the S_{DM} factor integral, comprising of a solid angle integral and an integral along the line of sight, as seen in eq. (3.1).

Each integral is performed as a Riemann sum: an integral is approximated as the sum of the function values on a grid, times the spacing between elements of such grid, as in:

$$\int_a^b f(x) dx \approx \sum_{i=1}^n f(x_i) \Delta x_i \quad (\text{A.1})$$

where $x_i \in [a, b]$, $\Delta x_i = \frac{x_{i+1} - x_{i-1}}{2}$

And the process is trivially extended for double and triple integrals. On the limit $n \rightarrow \infty$ both expressions are equivalent if x_i are evenly spaced between a and b.

This kind of approximations yield greater errors in areas where f changes rapidly and X_i evaluation points are scarce. Thus, it is critical for the accuracy of these algorithms to make a good choice of evaluation points X_i . We will start by analyzing the solid angle integral, and how it is possible to optimize the evaluation points for the Riemann sum.

First, spherical symmetry of the halo density profile can be used to evaluate the dependence on the azimuthal angle Φ :

$$\int_{\theta=0}^{\theta_{\max}} \int_{\Phi=0}^{2\pi} \bar{S}(\theta, \Phi) \sin \theta d\theta d\Phi = 2\pi \int_{\theta=0}^{\theta_{\max}} \bar{S}(\theta) . \quad (\text{A.2})$$

Then only remains to choose a suitable choice of evaluation points for θ . For circular shaped regions we chose logarithmically spaced points between $\theta \approx 10^{-6}$ arcsec and θ_{\max} (40 arcsec).⁸ This allows us to have a greater definition around the profile inner regions, where density is expected to change rapidly. Logarithmic spacing was also used for ‘donut’ shaped regions mentioned in section 3.1.

A more complex analysis is required for the integral along the line of sight:

$$\bar{S}(\theta, \Phi) = \int_{x=0}^{x=\infty} \rho(r(x, \theta, \Phi)) dx . \quad (\text{A.3})$$

Here we find the same challenge in evaluation points: it is necessary to have tightly packed points around the x values closer to the GC. But other numerical problems arise in the definition of r :

$$r = \sqrt{r_{\text{GC}}^2 + x^2 - 2xr_{\text{GC}} \cos \theta} . \quad (\text{A.4})$$

Where r_{GC} is the distance between the Sun and the GC ($\approx 8 \times 10^3$ pc). If parameters are such that we can access the inner regions of the halo profile ($\approx 10^{-7}$ pc), then this result is to be acquired from the subtraction of two similar quantities up to 10^{-14} kpc²: ($r_{\text{GC}}^2 + x^2$) and $2xr_{\text{GC}} \cos \theta$. This would have resulted in floating point precision errors for ordinary data storage types. Then, it was necessary to find an expression for $r(x, \theta)$ that remained accurate on such scales.

So, we first redefine the zero of the x coordinate, so it is measured from the closest point to the GC, as shown in fig. 11. Then, for small theta the expression in eq. (A.4) can be

⁸The lower angle corresponds to the shortest relevant radius for RAR profiles.

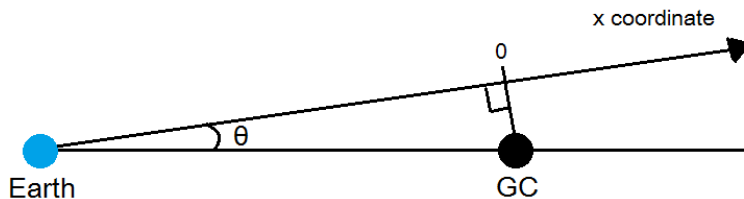


Figure 11. Coordinate system election schematic. $x - \theta$ plane slice. X coordinate zero is set at the axis' closest point to the GC.

approximated as:

$$r^2 = r_{\text{GC}}^2 \left(-2\epsilon(\theta) + \left(\frac{x}{r_{\text{GC}}} \right)^2 - 4 \frac{x}{r_{\text{GC}}} \epsilon(\theta) \right)$$

$$\text{where } \epsilon(\theta) = \cos \theta - 1 = -\frac{\theta^2}{2} + \frac{\theta^4}{24} - \dots \quad (\text{A.5})$$

Where, for small θ and positive x it involves sums of positive expressions only.

Using this new definition of the x coordinate origin, we can solve the sampling problem using logarithmic spaced evaluation points around $x=0$. This kind of spacing was used on the intervals $X = [-r_{\text{GC}}, -10^{-7}]$ and $X = [10^{-7}, 2r_{\text{halo}}]$, with r_{halo} the MW DM halo radius (≈ 55 kpc). Then, Riemann sums were executed to evaluate the integral on these points using eq. (A.5).

B A sterile neutrino production mechanism: V-boson decay

The required Decay rate of a V -boson decaying into two sterile neutrinos, in view of the interaction term (5.2) is given by the standard formula:

$$\Gamma = \frac{\mathcal{S}}{2E} \left[\int \prod_{i=1}^m \frac{d^3 p'_i}{2E'_i (2\pi)^3} \right] |\overline{\mathcal{M}}|^2 (2\pi)^4 \delta^{(4)} \left(\sum_{i=1}^m p'_i - p \right), \quad (\text{B.1})$$

where p (p'_i , $i = 1, \dots, m$) denote the four- momenta of the decaying particle (decay products), \mathcal{S} is a statistical factor that equals $1/(n!)$ for each group of n identical particles in the decay products, and $|\overline{\mathcal{M}}|^2$ is the square of the matrix element between initial and final states, averaged over initial-spin states and summed over final-spin ones.

For the evaluation of the amplitude \mathcal{M} we use the Feynman rule for the vertex $V_\mu \bar{\nu}_1 \nu_1$

$$-ig_V \gamma^\mu \left(\frac{1 + \gamma_5}{2} \right). \quad (\text{B.2})$$

To evaluate the decay width (B.1) we use the following Casimir identities (in the following expressions, $u_a(p)$ ($v_b(p)$) denote polarization spinors (antispinors) appearing in the solution

of the free Dirac (or Majorana) equations):

$$\begin{aligned}
& \sum_{i_A, i_B = \uparrow, \downarrow} \left(\bar{u}^{(i_A)}(p_A) \Gamma_I u^{(i_B)}(p_B) \right)^\dagger \left(\bar{u}^{(i_A)}(p_A) \Gamma_{II} u^{(i_B)}(p_B) \right) \\
&= \text{Tr} \left[\bar{\Gamma}_I \left(\gamma^\mu p_{A\mu} + m_A \right) \Gamma_{II} \left(\gamma^\mu p_{B\mu} + m_B \right) \right], \\
& \sum_{i_A, i_B = \uparrow, \downarrow} \left(\bar{v}^{(i_A)}(p_A) \Gamma_I u^{(i_B)}(p_B) \right)^\dagger \left(\bar{v}^{(i_A)}(p_A) \Gamma_{II} u^{(i_B)}(p_B) \right) \\
&= \text{Tr} \left[\bar{\Gamma}_I \left(\gamma^\mu p_{A\mu} - m_A \right) \Gamma_{II} \left(\gamma^\mu p_{B\mu} + m_B \right) \right], \\
& \sum_{i_A, i_B = \uparrow, \downarrow} \left(\bar{v}^{(i_A)}(p_A) \Gamma_I v^{(i_B)}(p_B) \right)^\dagger \left(\bar{v}^{(i_A)}(p_A) \Gamma_{II} v^{(i_B)}(p_B) \right) \\
&= \text{Tr} \left[\bar{\Gamma}_I \left(\gamma^\mu p_{A\mu} - m_A \right) \Gamma_{II} \left(\gamma^\mu p_{B\mu} - m_B \right) \right], \tag{B.3}
\end{aligned}$$

for any two 4×4 matrices Γ_I, Γ_{II} , where $\bar{\Gamma}_I \equiv \gamma^0 \Gamma_I^\dagger \gamma^0$, with γ^μ the 4×4 Dirac γ -matrices. For our purposes it suffices to calculate the width (B.1) in flat Minkowski space time. In this case, we have the properties

$$\{\gamma^\mu, \gamma^\nu\} = 2\eta^{\mu\nu} \mathbf{1} \tag{B.4}$$

$$\{\gamma^\mu, \gamma^5\} = 0 \tag{B.5}$$

$$\bar{\gamma}^\mu \equiv \gamma^0 (\gamma^\mu)^\dagger \gamma^0 = \gamma^\mu \tag{B.6}$$

$$\overline{\gamma^\mu \gamma^5} \equiv \gamma^0 (\gamma^\mu \gamma^5)^\dagger \gamma^0 = \gamma^\mu \gamma^5 \tag{B.7}$$

$$\text{Tr}[\mathbf{1}] = 4 \tag{B.8}$$

$$\text{Tr}(\gamma^\mu \gamma^\nu) = 4\eta^{\mu\nu} \tag{B.9}$$

$$\text{Tr}(\gamma^\mu \gamma^\lambda \gamma^\nu \gamma^\rho) = 4(\eta^{\mu\lambda} \eta^{\nu\rho} - \eta^{\mu\nu} \eta^{\lambda\rho} + \eta^{\mu\rho} \eta^{\nu\lambda}) \tag{B.10}$$

where $\gamma^5 = i\gamma^0 \gamma^1 \gamma^2 \gamma^3$, the trace Tr is over spinor indices, $\mathbf{1}$ denotes the 4×4 identity matrix in spinor space and $\eta^{\mu\nu}$ is the Minkowski metric with the signature convention $(+, -, -, -)$. Note that the trace $\text{Tr}(\gamma^\mu \gamma^\nu \gamma^5) = 0$ while $\text{Tr}(\gamma^\mu \gamma^\lambda \gamma^\nu \gamma^\rho \gamma^5)$ is totally antisymmetric in the Lorentz indices.

Since the phenomenological considerations of [90] require the vector boson mass m_V to be much larger (at least four orders of magnitude) than the sterile neutrino DM mass m , $m_V \gg m$, we may treat the fermionic product of the decay $V_\mu \bar{\nu}_1 \nu_1$ as *practically massless*. Hence, applying the identities of eq. (B.3) in this case, yields:

$$-i\mathcal{M} = \epsilon_W^\mu(p) \bar{u}_{f_1}^{(i_1)}(p_1) (-ig_V \gamma_\mu) \left(\frac{1 + \gamma^5}{2} \right) v_{f_2}^{(i_2)}(p_2), \tag{B.11}$$

where ϵ_V^μ is the polarisation of the massive V -boson. and $f_{1,2}$ denote the fermionic decay products in the three processes. The fermions f_i are all massless. The square of the initial-spin-averaged and final-spin-summed amplitude entering eq. (B.1) reads:

$$|\overline{\mathcal{M}}|^2 = \frac{1}{3} \sum_{i_1, i_2 = \uparrow, \downarrow} |\mathcal{M}|^2, \tag{B.12}$$

where the factor $1/3$ is due to the fact that we have $2s + 1$ (with $s = 1$) initial spins of the massive vector boson to average over. Taking into account the identities of eq. (B.3),

with the matrices Γ_I, Γ_{II} being γ^μ, γ^ν and $\gamma^\mu \gamma^5, \gamma^\nu \gamma^5$, as well as the fact that the sum over vector-boson- V polarisation (spin) states is

$$\sum_{\text{spin}} \epsilon_\mu(p) \epsilon_\nu(p) = -\eta_{\mu\nu} + \frac{p_\mu p_\nu}{m_V^2},$$

we may evaluate the amplitude (B.12) as (from now on we omit the particle-species index from the polarisation tensors of spinors for simplicity)

$$\begin{aligned} |\overline{\mathcal{M}}|^2 &= \frac{g_V^2}{3} \sum_{i_1, i_2 = \uparrow, \downarrow} \left[\bar{u}^{(i_1)}(p'_1) \gamma_\mu \frac{1 + \gamma^5}{2} v^{(i_2)}(p'_2) \right]^\dagger \\ &\quad \left[\bar{u}^{(i_1)}(p'_1) \gamma_\nu \frac{1 + \gamma^5}{2} v^{(i_2)}(p'_2) \right] \epsilon_V^\mu(p) \epsilon_V^\nu(p) \\ &= \frac{g_V^2}{3} \text{Tr} \left[\gamma_\mu \frac{1 + \gamma^5}{2} (\gamma_\rho p_2'^\rho) \gamma_\nu \frac{1 + \gamma^5}{2} \gamma_\sigma p_1'^\sigma \right] \\ &\quad \times \left(-\eta^{\mu\nu} + \frac{p_V^\mu p_V^\nu}{m_V^2} \right) \\ &= \frac{g_V^2}{6} \text{Tr} [\gamma_\mu (1 + \gamma^5) \gamma_\rho \gamma_\nu \gamma_\sigma] p_2'^\rho p_1'^\sigma \left(-\eta^{\mu\nu} + \frac{p_V^\mu p_V^\nu}{m_V^2} \right) \\ &= \frac{g_V^2}{6} \text{Tr} [\gamma_\mu \gamma_\rho \gamma_\nu \gamma_\sigma] p_2'^\rho p_1'^\sigma \left(-\eta^{\mu\nu} + \frac{p_V^\mu p_V^\nu}{m_V^2} \right). \end{aligned}$$

In the last simplification, we used the anti-commutation properties of γ^5 with γ_μ , and the fact that $\left(\frac{1+\gamma^5}{2}\right)^2 = \frac{1+\gamma^5}{2}$ and $\frac{1+\gamma^5}{2} \frac{1-\gamma^5}{2} = 0$. Above we also took into account that the trace containing γ^5 is zero because it gives rise to a totally antisymmetric tensor (rubric) which is contracted with a symmetric tensor with respect to the μ, ν , indices, $\left(-\eta^{\mu\nu} + \frac{p_V^\mu p_V^\nu}{m_V^2}\right)$. Using the identities of Dirac matrices, given previously, we then obtain

$$\begin{aligned} |\overline{\mathcal{M}}|^2 &= \frac{2g_V^2}{3} (p_{2\mu}' p_{1\nu}' + p_{2\nu}' p_{1\mu}' - \eta_{\mu\nu} p_1' \cdot p_2') \left(-\eta^{\mu\nu} + \frac{p_V^\mu p_V^\nu}{m_V^2} \right) \\ &= \frac{2g_V^2}{3} \left(p_2' \cdot p_1' + 2 \frac{p_2' \cdot p_1' \cdot p}{m_V^2} \right) \end{aligned} \quad (\text{B.13})$$

where we used the on-shell condition for the V momentum $p^\mu \eta_{\mu\nu} p^\nu = m_V^2$. Using the conservation of energy momentum in the vertex (p incoming, p_1', p_2' outgoing),

$$p^\mu - p_1'^\mu - p_2'^\mu = 0, \quad (\text{B.14})$$

we square it (in a covariant way) to derive :

$$\begin{aligned} 0 &= p_2' \cdot p_2' + p \cdot p + p_1' \cdot p_1' + 2p_2' \cdot p_1' - 2p \cdot (p_2' + p_1') \\ &= m_W^2 + 2p_2' \cdot p_1' - 2p \cdot p = -m_W^2 + 2p_2' \cdot p_1' \\ &\Rightarrow p_2' \cdot p_1' = m_W^2/2 \end{aligned}$$

where we used the on-shell conditions (in our conventions for the metric $(+1, -1, -1, -1)$)

$$p \cdot p = m_V^2, \quad p'_1 \cdot p'_1 = 0, \quad p'_2 \cdot p'_2 = 0.$$

In a similar way by writing the square as

$$\begin{aligned} 0 &= p'_2 \cdot p'_2 + p \cdot p + p'_1 \cdot p'_1 - 2p'_1 \cdot (p - p'_2) - 2p \cdot p'_2 \\ &= p'_2 \cdot p'_2 + p \cdot p - p'_1 \cdot p'_1 - 2p \cdot p'_2 \\ &\Rightarrow p \cdot p'_2 = m_V^2/2. \end{aligned}$$

And finally, by writing the square as:

$$\begin{aligned} 0 &= p'_2 \cdot p'_2 + p \cdot p + p'_1 \cdot p'_1 - 2p'_2 \cdot (p - p'_1) - 2p'_1 \cdot p \\ &= m_W^2 - 2p'_2 \cdot p'_2 - 2p \cdot p'_1 \\ &\Rightarrow p'_1 \cdot p = m_V^2/2. \end{aligned}$$

Then, the amplitude can be written in terms of masses

$$|\overline{\mathcal{M}}|^2 = \frac{2g_V^2}{3} m_V^2. \quad (\text{B.15})$$

In the rest frame of the V -boson ($E_V = m_V$, $\mathbf{p}_V = 0$) the phase space integration in eq. (B.1) is done by first performing the spatial delta function integration

$$\int d^3p'_2 \delta^{(3)}(-\mathbf{p}'_1 - \mathbf{p}'_2),$$

which simply implies that the spatial momenta of the decay products (which are massless particles) are equal in magnitude $|\mathbf{p}'_1| = |\mathbf{p}'_2|$.

In the case of Majorana sterile neutrinos, there is one group of two ($n = 2$) identical particles in the products of the V -vector-boson decay so the statistical factor \mathcal{S} in the definition of the width (B.1) is $\mathcal{S} = \frac{1}{2}$ (for Dirac type “inos” $\mathcal{S} = 1$, as in that case there are no identical particles among the decay products). Treating the neutrino as practically massless inside the phase-space integration, which suffices for our approximate discussion here, we then obtain:

$$\begin{aligned} \Gamma &= \frac{1}{16 m_V} \int 4\pi |\mathbf{p}'_2|^2 d|\mathbf{p}'_2| \delta(M_V - 2|\mathbf{p}'_2|) \frac{1}{4\pi^2 |\mathbf{p}'_2|^2} |\overline{\mathcal{M}}|^2 \\ &= \frac{1}{32 \pi m_V} |\overline{\mathcal{M}}|^2 \simeq \frac{g_V^2}{48 \pi} m_V \end{aligned} \quad (\text{B.16})$$

where we used that $\int d|\mathbf{p}'_2| \delta(m_V - 2|\mathbf{p}'_2|) = \frac{1}{2}$.

References

- [1] G. Jungman, M. Kamionkowski and K. Griest, *Supersymmetric dark matter*, *Phys. Rept.* **267** (1996) 195 [[hep-ph/9506380](#)].
- [2] L. Bergström, *Nonbaryonic dark matter: Observational evidence and detection methods*, *Rept. Prog. Phys.* **63** (2000) 793 [[hep-ph/0002126](#)].
- [3] C. Munoz, *Dark matter detection in the light of recent experimental results*, *Int. J. Mod. Phys.* **A19** (2004) 3093 [[hep-ph/0309346](#)].

- [4] G. Bertone, D. Hooper and J. Silk, *Particle dark matter: Evidence, candidates and constraints*, *Phys. Rept.* **405** (2005) 279 [[hep-ph/0404175](#)].
- [5] Z. G. Berezhiani and R. N. Mohapatra, *Reconciling present neutrino puzzles: Sterile neutrinos as mirror neutrinos*, *Phys. Rev. D* **52** (1995) 6607.
- [6] E. Jin Chun and H. B. Kim, *Nonthermal axino as cool dark matter in the supersymmetric standard model without r parity*, *Phys. Rev. D* **60** (1999) 095006.
- [7] P. Langacker, *Mechanism for ordinary-sterile neutrino mixing*, *Phys. Rev. D* **58** (1998) 093017.
- [8] N. Arkani-Hamed, S. Dimopoulos, G. Dvali and J. March-Russell, *Neutrino masses from large extra dimensions*, *Phys. Rev. D* **65** (2001) 024032.
- [9] K. N. Abazajian, G. M. Fuller and M. Patel, *Cosmological constraints on bulk neutrinos*, *Phys. Rev. Lett.* **90** (2003) 061301.
- [10] T. Asaka, S. Blanchet and M. Shaposhnikov, *The ν msm, dark matter and neutrino masses*, *Physics Letters B* **631** (2005) 151 .
- [11] THE K2K COLLABORATION collaboration, E. Aliu et al., *Evidence for muon neutrino oscillation in an accelerator-based experiment*, *Phys. Rev. Lett.* **94** (2005) 081802.
- [12] SNO COLLABORATION collaboration, Ahmad et al., *Direct evidence for neutrino flavor transformation from neutral-current interactions in the sudbury neutrino observatory*, *Phys. Rev. Lett.* **89** (2002) 011301.
- [13] SUPER-KAMIOKANDE COLLABORATION collaboration, Y. Ashie et al., *Measurement of atmospheric neutrino oscillation parameters by super-kamiokande i*, *Phys. Rev. D* **71** (2005) 112005.
- [14] KAMLAND COLLABORATION collaboration, T. Araki et al., *Measurement of neutrino oscillation with kamland: Evidence of spectral distortion*, *Phys. Rev. Lett.* **94** (2005) 081801.
- [15] C. Weinheimer, *Direct neutrino mass experiments - present and future*, *Nuclear Physics B - Proceedings Supplements* **118** (2003) 279 .
- [16] D. Eichler, *TeV particles as weakly unstable dark matter*, *Phys. Rev. Lett.* **63** (1989) 2440.
- [17] E. Nardi, F. Sannino and A. Strumia, *Decaying dark matter can explain the e^\pm excesses*, *J. Cosmology Astropart. Phys.* **1** (2009) 043 [[0811.4153](#)].
- [18] Arvanitaki et al., *Astrophysical probes of unification*, *Phys. Rev. D* **79** (2009) 105022.
- [19] K. Hamaguchi, S. Shirai and T. Yanagida, *Cosmic ray positron and electron excess from hidden-fermion dark matter decays*, *Physics Letters B* **673** (2009) 247 .
- [20] W. Buchmüller, L. Covi, K. Hamaguchi, A. Ibarra and T. T. Yanagida, *Gravitino dark matter in r -parity breaking vacua*, *Journal of High Energy Physics* **2007** (2007) 037.
- [21] S.-L. Chen, R. N. Mohapatra, S. Nussinov and Y. Zhang, *R -parity breaking via type ii seesaw, decaying gravitino dark matter and pamelas positron excess*, *Physics Letters B* **677** (2009) 311 .
- [22] A. Ibarra, A. Ringwald, D. Tran and C. Weniger, *Cosmic rays from leptophilic dark matter decay via kinetic mixing*, *Journal of Cosmology and Astroparticle Physics* **2009** (2009) 017.
- [23] P. F. Pérez and S. Spinner, *Spontaneous r -parity breaking in supersymmetric models*, *Phys. Rev. D* **80** (2009) 015004.
- [24] S. Shirai, F. Takahashi and T. Yanagida, *R -violating decay of wino dark matter and electron/positron excesses in the pamelas/fermi experiments*, *Physics Letters B* **680** (2009) 485 .
- [25] C.-R. Chen, F. Takahashi and T. Yanagida, *Gamma rays and positrons from a decaying hidden gauge boson*, *Physics Letters B* **671** (2009) 71 .

- [26] A. Ibarra, A. Ringwald and C. Weniger, *Hidden gauginos of an unbroken $u(1)$: cosmological constraints and phenomenological prospects*, *Journal of Cosmology and Astroparticle Physics* **2009** (2009) 003.
- [27] A. Ibarra and D. Tran, *Gamma-ray spectrum from gravitino dark matter decay*, *Phys. Rev. Lett.* **100** (2008) 061301.
- [28] A. Ibarra and D. Tran, *Antimatter signatures of gravitino dark matter decay*, *Journal of Cosmology and Astroparticle Physics* **2008** (2008) 002.
- [29] K. Ishiwata, S. Matsumoto and T. Moroi, *High energy cosmic rays from the decay of gravitino dark matter*, *Phys. Rev. D* **78** (2008) 063505.
- [30] M. Pospelov and M. Trott, *R -parity preserving super-wimp decays*, *Journal of High Energy Physics* **2009** (2009) 044.
- [31] K. J. Bae and B. Kyae, *Pamela/atic anomaly from exotic mediated dark matter decay*, *Journal of High Energy Physics* **2009** (2009) 102.
- [32] K. Cheung, P.-Y. Tseng and T.-C. Yuan, *Double-action dark matter, pamela and atic*, *Physics Letters B* **678** (2009) 293 .
- [33] H. Fukuoka, J. Kubo and D. Suematsu, *Anomaly induced dark matter decay and pamela/atic experiments*, *Physics Letters B* **678** (2009) 401 .
- [34] A. Ibarra, D. Tran and C. Weniger, *Decaying dark matter in light of the pamela and fermi lat data*, *Journal of Cosmology and Astroparticle Physics* **2010** (2010) 009.
- [35] L. Covi, M. Grefe, A. Ibarra and D. Tran, *Unstable gravitino dark matter and neutrino flux*, *Journal of Cosmology and Astroparticle Physics* **2009** (2009) 029.
- [36] J. Hisano, M. Kawasaki, K. Kohri and K. Nakayama, *Neutrino signals from annihilating/decaying dark matter in the light of recent measurements of cosmic ray electron/positron fluxes*, *Phys. Rev. D* **79** (2009) 043516.
- [37] J. Liu, P.-f. Yin and S.-h. Zhu, *Prospects for detecting neutrino signals from annihilating/decaying dark matter to account for the pamela and atic results*, *Phys. Rev. D* **79** (2009) 063522.
- [38] J. Hisano, K. Nakayama and M. J. Yang, *Upward muon signals at neutrino detectors as a probe of dark matter properties*, *Physics Letters B* **678** (2009) 101 .
- [39] M. R. Buckley, D. Spolyar, K. Freese, D. Hooper and H. Murayama, *High-energy neutrino signatures of dark matter*, *Phys. Rev. D* **81** (2010) 016006.
- [40] P.-f. Yin, Q. Yuan, J. Liu, J. Zhang, X.-j. Bi, S.-h. Zhu et al., *Pamela data and leptonicly decaying dark matter*, *Phys. Rev. D* **79** (2009) 023512.
- [41] B. Kyae, *Pamela/atic anomaly from the meta-stable extra dark matter component and the leptophilic yukawa interaction*, *Journal of Cosmology and Astroparticle Physics* **2009** (2009) 028.
- [42] D. m. c. A. Demir, L. L. Everett, M. Frank, L. Selbuz and I. Turan, *Sneutrino dark matter: Symmetry protection and cosmic ray anomalies*, *Phys. Rev. D* **81** (2010) 035019.
- [43] A. Ibarra and D. Tran, *Decaying dark matter and the pamela anomaly*, *Journal of Cosmology and Astroparticle Physics* **2009** (2009) 021.
- [44] A. D. Dolgov and S. H. Hansen, *Massive sterile neutrinos as warm dark matter*, *Astroparticle Physics* **16** (2002) 339 [[hep-ph/0009083](#)].
- [45] P. B. Pal and L. Wolfenstein, *Radiative decays of massive neutrinos*, *Phys. Rev. D* **25** (1982) 766.

- [46] K. N. Abazajian, M. Markevitch, S. M. Koushiappas and R. C. Hickox, *Limits on the radiative decay of sterile neutrino dark matter from the unresolved cosmic and soft x-ray backgrounds*, *Phys. Rev. D* **75** (2007) 063511.
- [47] G. Bertone, *Particle Dark Matter : Observations, Models and Searches*. Cambridge University Press, 2010.
- [48] R. Adhikari, M. Agostini, N. A. Ky, T. Araki, M. Archidiacono, M. Bahr et al., *A White Paper on keV sterile neutrino Dark Matter*, *Journal of Cosmology and Astroparticle Physics* **1** (2017) 025 [1602.04816].
- [49] K. Perez, K. C. Y. Ng, J. F. Beacom, C. Hersh, S. Horiuchi and R. Krivonos, *Almost closing the ν MSM sterile neutrino dark matter window with NuSTAR*, *Phys. Rev.* **D95** (2017) 123002 [1609.00667].
- [50] S. Dodelson and L. M. Widrow, *Sterile-neutrinos as dark matter*, *Phys. Rev. Lett.* **72** (1994) 17 [hep-ph/9303287].
- [51] T. Asaka, M. Laine and M. Shaposhnikov, *Lightest sterile neutrino abundance within the nuMSM*, *JHEP* **01** (2007) 091 [hep-ph/0612182].
- [52] M. Laine and M. Shaposhnikov, *Sterile neutrino dark matter as a consequence of nuMSM-induced lepton asymmetry*, *JCAP* **0806** (2008) 031 [0804.4543].
- [53] X.-D. Shi and G. M. Fuller, *A New dark matter candidate: Nonthermal sterile neutrinos*, *Phys. Rev. Lett.* **82** (1999) 2832 [astro-ph/9810076].
- [54] A. Boyarsky, O. Ruchayskiy and D. Iakubovskiy, *A Lower bound on the mass of Dark Matter particles*, *JCAP* **0903** (2009) 005 [0808.3902].
- [55] S. Horiuchi, P. J. Humphrey, J. Onorbe, K. N. Abazajian, M. Kaplinghat and S. Garrison-Kimmel, *Sterile neutrino dark matter bounds from galaxies of the Local Group*, *Phys. Rev.* **D89** (2014) 025017 [1311.0282].
- [56] A. Schneider, *Astrophysical constraints on resonantly produced sterile neutrino dark matter*, *JCAP* **1604** (2016) 059 [1601.07553].
- [57] J. F. Navarro, C. S. Frenk and S. D. White, *The Structure of cold dark matter halos*, *Astrophys.J.* **462** (1996) 563 [astro-ph/9508025].
- [58] J. F. Navarro, C. S. Frenk and S. D. White, *A Universal density profile from hierarchical clustering*, *Astrophys.J.* **490** (1997) 493 [astro-ph/9611107].
- [59] B. Moore, T. Quinn, F. Governato, J. Stadel and G. Lake, *Cold collapse and the core catastrophe*, *Monthly Notices of the Royal Astronomical Society* **310** (1999) 1147.
- [60] A. Klypin, A. V. Kravtsov, J. Bullock and J. Primack, *Resolving the structure of cold dark matter halos*, *Astrophys.J.* **554** (2001) 903 [astro-ph/0006343].
- [61] J. F. Navarro et al., *The Inner structure of Lambda-CDM halos 3: Universality and asymptotic slopes*, *Mon.Not.Roy.Astron.Soc.* **349** (2004) 1039 [astro-ph/0311231].
- [62] A. Boyarsky, O. Ruchayskiy and M. Shaposhnikov, *The Role of sterile neutrinos in cosmology and astrophysics*, *Ann. Rev. Nucl. Part. Sci.* **59** (2009) 191 [0901.0011].
- [63] A. Boyarsky, D. Iakubovskiy and O. Ruchayskiy, *Next decade of sterile neutrino studies*, *Physics of the Dark Universe* **1** (2012) 136 [1306.4954].
- [64] A. Schneider, R. E. Smith, A. V. Macciò and B. Moore, *Non-linear evolution of cosmological structures in warm dark matter models*, *MNRAS* **424** (2012) 684 [1112.0330].
- [65] S. Bose, W. A. Hellwing, C. S. Frenk, A. Jenkins, M. R. Lovell, J. C. Helly et al., *Substructure and galaxy formation in the Copernicus Complexio warm dark matter simulations*, *MNRAS* **464** (2017) 4520 [1604.07409].

- [66] D. Merritt, A. W. Graham, B. Moore, J. Diemand and B. Terzić, *Empirical models for dark matter halos. i. nonparametric construction of density profiles and comparison with parametric models*, *The Astronomical Journal* **132** (2006) 2685.
- [67] A. Burkert, *The structure of dark matter halos in dwarf galaxies*, *The Astrophysical Journal Letters* **447** (1995) L25.
- [68] R. Ruffini, C. R. Argüelles and J. A. Rueda, *On the core-halo distribution of dark matter in galaxies*, *Monthly Notices of the Royal Astronomical Society* **451** (2015) 622.
- [69] C. R. Argüelles, A. Krut, J. A. Rueda and R. Ruffini, *Novel constraints on fermionic dark matter from galactic observables I: The Milky Way*, *Physics of the Dark Universe* **21** (2018) 82 [[1606.07040](#)].
- [70] V. Barger, R. Phillips and S. Sarkar, *Remarks on the karmen anomaly*, *Physics Letters B* **352** (1995) 365 .
- [71] A. Boyarsky, D. Malyshev, A. Neronov and O. Ruchayskiy, *Constraining DM properties with SPI*, *Mon. Not. Roy. Astron. Soc.* **387** (2008) 1345 [[0710.4922](#)].
- [72] K. C. Y. Ng, S. Horiuchi, J. M. Gaskins, M. Smith and R. Preece, *Improved Limits on Sterile Neutrino Dark Matter using Full-Sky Fermi Gamma-Ray Burst Monitor Data*, *Phys. Rev.* **D92** (2015) 043503 [[1504.04027](#)].
- [73] S. Riemer-Sørensen et al., *Dark matter line emission constraints from NuSTAR observations of the Bullet Cluster*, *Astrophys. J.* **810** (2015) 48 [[1507.01378](#)].
- [74] A. Neronov, D. Malyshev and D. Eckert, *Decaying dark matter search with NuSTAR deep sky observations*, *Phys. Rev.* **D94** (2016) 123504 [[1607.07328](#)].
- [75] J. I. Read, *The Local Dark Matter Density*, *J. Phys.* **G41** (2014) 063101 [[1404.1938](#)].
- [76] F. Calore, N. Bozorgnia, M. Lovell, G. Bertone, M. Schaller, C. S. Frenk et al., *Simulated Milky Way analogues: implications for dark matter indirect searches*, *JCAP* **1512** (2015) 053 [[1509.02164](#)].
- [77] A. V. Patwardhan, G. M. Fuller, C. T. Kishimoto and A. Kusenko, *Diluted equilibrium sterile neutrino dark matter*, *Phys. Rev. D* **92** (2015) 103509 [[1507.01977](#)].
- [78] A. Boyarsky, J. Lesgourgues, O. Ruchayskiy and M. Viel, *Lyman- α constraints on warm and on warm-plus-cold dark matter models*, *"JCAP"* **5** (2009) 012 [[0812.0010](#)].
- [79] C. Yèche, N. Palanque-Delabrouille, J. Baur and H. du Mas des Bourboux, *Constraints on neutrino masses from Lyman-alpha forest power spectrum with BOSS and XQ-100*, *"JCAP"* **6** (2017) 047 [[1702.03314](#)].
- [80] S. Gillessen, F. Eisenhauer, T. K. Fritz, H. Bartko, K. Dodds-Eden, O. Pfuhl et al., *The Orbit of the Star S2 Around SGR A* from Very Large Telescope and Keck Data*, *Astrophysical Journal Letters* **707** (2009) L114 [[0910.3069](#)].
- [81] Y. Sofue, *Rotation Curve and Mass Distribution in the Galactic Center - From Black Hole to Entire Galaxy*, *Public. of the Astron. Soc. of Japan* **65** (2013) 118 [[1307.8241](#)].
- [82] K. Mori et al., *NuSTAR Hard X-ray Survey of the Galactic Center Region. I. Hard X-ray Morphology and Spectroscopy of the Diffuse Emission*, *Astrophys. J.* **814** (2015) 94 [[1510.04631](#)].
- [83] C. J. Hailey et al., *Evidence for intermediate polars as the origin of the Galactic Center hard X-ray emission*, *Astrophys. J.* **826** (2016) 160 [[1605.06066](#)].
- [84] A. Boyarsky, A. Neronov, O. Ruchayskiy, M. Shaposhnikov and I. Tkachev, *Where to find a dark matter sterile neutrino?*, *Phys. Rev. Lett.* **97** (2006) 261302 [[astro-ph/0603660](#)].
- [85] K. Koyama, H. Awaki, H. Kunieda, S. Takano and Y. Tawara, *Intense 6.7-keV iron line emission from the Galactic Centre*, *Nature* **339** (1989) 603.

- [86] K. Koyama, Y. Maeda, T. Sonobe, T. Takeshima, Y. Tanaka and S. Yamauchi, *ASCA View of Our Galactic Center: Remains of Past Activities in X-Rays?*, *Publications of the Astronomical Society of Japan* **48** (1996) 249.
- [87] D. R. Wik et al., *NuSTAR Observations of the Bullet Cluster: Constraints on Inverse Compton Emission*, *Astrophys. J.* **792** (2014) 48 [[1403.2722](#)].
- [88] S. Y. Kim, A. H. G. Peter and J. R. Hargis, *There is No Missing Satellites Problem*, *ArXiv e-prints* (2017) [[1711.06267](#)].
- [89] M. Shaposhnikov, *The nuMSM, leptonic asymmetries, and properties of singlet fermions*, *JHEP* **08** (2008) 008 [[0804.4542](#)].
- [90] C. R. Argüelles, N. E. Mavromatos, J. A. Rueda and R. Ruffini, *The role of self-interacting right-handed neutrinos in galactic structure*, *JCAP* **1604** (2016) 038 [[1502.00136](#)].
- [91] J. S. Bullock and M. Boylan-Kolchin, *Small-Scale Challenges to the Λ CDM Paradigm*, *ARA&A* **55** (2017) 343 [[1707.04256](#)].
- [92] N. E. Mavromatos and A. Pilaftsis, *Anomalous Majorana Neutrino Masses from Torsionful Quantum Gravity*, *Phys. Rev.* **D86** (2012) 124038 [[1209.6387](#)].
- [93] M. Drewes and J. U. Kang, *Sterile neutrino Dark Matter production from scalar decay in a thermal bath*, *JHEP* **05** (2016) 051 [[1510.05646](#)].
- [94] F. Bezrukov, A. Chudaykin and D. Gorbunov, *Hiding an elephant: heavy sterile neutrino with large mixing angle does not contradict cosmology*, *JCAP* **1706** (2017) 051 [[1705.02184](#)].
- [95] P. Minkowski, *$\mu \rightarrow e\gamma$ at a rate of one out of 10^9 muon decays?*, *Physics Letters B* **67** (1977) 421.
- [96] R. N. Mohapatra and G. Senjanovic, *Neutrino mass and spontaneous parity nonconservation*, *Physical Review Letters* **44** (1980) 912.
- [97] J. Schechter and J. W. F. Valle, *Neutrino masses in $SU(2) \otimes U(1)$ theories*, *Phys. Rev. D* **22** (1980) 2227.
- [98] G. Lazarides, Q. Shafi and C. Wetterich, *Proton lifetime and fermion masses in an $SO(10)$ model*, *Nuclear Physics B* **181** (1981) 287.
- [99] M. Gell-Mann, P. Ramond and R. Slansky, in *Supergravity*, eds. D.Z. Freedman and P. van Nieuwenhuizen (North-Holland, Amsterdam, 1979).
- [100] T. Yanagida, in *Proc. of the Workshop on the Unified Theory and the Baryon Number in the Universe*, Tsukuba, Japan, 1979, eds. O. Sawada and A. Sugamoto.
- [101] I. Siutsou, C. R. Argüelles and R. Ruffini, *Dark matter massive fermions and Einasto profiles in galactic haloes*, *Astronomy Reports* **59** (2015) 656 [[1402.0695](#)].
- [102] C. R. Argüelles, R. Ruffini, I. Siutsou and B. Fraga, *On the distribution of dark matter in galaxies: Quantum treatments*, *Journal of Korean Physical Society* **65** (2014) 801 [[1402.0700](#)].
- [103] N. E. Mavromatos, C. R. Argüelles, R. Ruffini and J. A. Rueda, *Self-interacting dark matter*, *International Journal of Modern Physics D* **26** (2017) 1730007.
- [104] D. Harvey, R. Massey, T. Kitching, A. Taylor and E. Tittley, *The non-gravitational interactions of dark matter in colliding galaxy clusters*, *Science* **347** (2015) 1462 [[1503.07675](#)].
- [105] E. W. Kolb and M. S. Turner, *The Early Universe*, *Front. Phys.* **69** (1990) 1.
- [106] J. Martin and C. Ringeval, *First CMB Constraints on the Inflationary Reheating Temperature*, *Phys. Rev.* **D82** (2010) 023511 [[1004.5525](#)].
- [107] M. Drewes, *What can the CMB tell about the microphysics of cosmic reheating?*, *JCAP* **1603** (2016) 013 [[1511.03280](#)].

- [108] M. Nemevsek, G. Senjanovic and Y. Zhang, *Warm Dark Matter in Low Scale Left-Right Theory*, *JCAP* **1207** (2012) 006 [[1205.0844](#)].